



THE UNIVERSITY OF QUEENSLAND
A U S T R A L I A

Low Cost Embedded Passive Bistatic Radar Detection Testbed

by

Flynn Kelly
4741858
flynn.kelly@uqconnect.edu.au

School of Electrical Engineering and Computer Science,
University of Queensland

Submitted for the degree of Bachelor of Science (Honours)
in the division of Electrical Engineering

Flynn Kelly
flynn.kelly@uqconnect.edu.au

October 23, 2024

Professor Michael Bruenig
Head of School
School of Electrical Engineering and Computer Science
The University of Queensland
St Lucia, Queensland 4072

Dear Professor Bruenig,

In accordance with the requirements of the degree of Bachelor of Science (Honours) in the School of Electrical Engineering and Computer Science, I present the following thesis entitled

‘Low Cost Passive Bistatic Radar Detection Testbed’

This thesis was performed under the supervision of Professor Bialkowski(EECS). I declare that the work submitted in the thesis is my own, except as acknowledged in the text and footnotes, and that it has not previously been submitted for a degree at the University of Queensland or any other institution.

Yours sincerely,

Flynn Kelly

Acknowledgements

Acknowledgements: recognise those who have been instrumental in the completion of the project. Acknowledgements should include any professional editorial advice received including the name of the editor and a brief description of the service rendered.

SUPERVISOR, FRIENDS, ETC....

Abstract

Abstract: MINIMAL VIABLE PRODUCT OVERVIEW

broad need, specific need, response aim, response methods, key outcomes and implications.

Affordable and efficient passive radar based detection, tracking and situational awareness technology is increasing in demand in a range of sectors and academia. As software-defined radio (SDR) technology becomes more widespread and single-board computers (SBCs) continue to gain processing power, the possibility of deploying passive radar systems in an embedded, cost-effective manner has emerged as a critical area of research and commercial development. The growing need for such systems is particularly evident in scenarios where traditional, expensive PC hardware setups at remote receiver (RX) locations are impractical or cost-prohibitive. This has created a specific need for streamlined, scalable systems that can function independently and effectively in various environments.

In response to these demands, this project aims to design and implement a low-cost, embedded passive radar detection testbed prototype system that leverages a digital broadcast signal as an illuminator of opportunity. The chosen approach involves utilizing existing embedded IoT hardware in combination with established digital signal processing (DSP) techniques and radar filtering algorithms. This integrated solution is intended to form a single embedded Linux testbed capable of handling both signal sampling and processing, along with sampling networking thereby eliminating the reliance on costly and complex physical hardware at each RX location.

Key outcomes of this research include the successful detection of aerial vehicles within controlled environments, an analysis of the system's latency, and a comprehensive evaluation of the overall cost-effectiveness of the design. The implications of this work include offering valuable insights into the scalability and cost-quality balance that can be achieved in future passive radar system implementations. Moreover, the project aims to deliver a re-usable, scaleable testbed which can be used to further develop and test passive radar based detection and situational awareness systems.

Contents

Acknowledgements	2
Abstract	3
List of Figures	6
List of Tables	7
1 Introduction	8
1.1 Topic and Relevance	8
1.2 Aims and Objectives	8
1.3 Scope	9
2 Background	10
2.1 Passive Radar Fundamentals	10
2.2 Illuminators of Opportunity	12
2.2.1 Radar and the Radio Frequency Spectrum	12
2.2.2 Key Parameters for Illuminators of Opportunity	13
2.2.3 Utility of Digital Illuminators	13
2.3 Range Doppler Mapping	16
2.4 Radio Hardware	17
2.4.1 Software Defined Radio	17
2.4.2 Antenna	18
2.5 Digital Signal Processing	19
2.6 IoT Architecture	21
2.7 Networking with Embedded Hardware	22
2.7.1 USB Drive Transfer	23
2.7.2 SSH	23
2.7.3 Ethernet	23
2.7.4 TCP Socket	23
2.7.5 Cloud Service	24
3 Literature Review	25
3.1 Low Cost IoT Hardware PBR Reciver Design	25
3.2 Illuminators of Opportunity	26
3.3 Existing Commercial Technology	27

4 Methodology and Design	28
4.1 Hardware	28
4.1.1 Software Defined Radio	28
4.1.2 Embedded Computing Platform	31
4.1.3 NVME Based Storage	32
4.1.4 Antenna Configuration	32
4.1.5 Testbed Design	33
4.2 Software	34
4.2.1 SDR Software	34
4.2.2 Networking Requirements	36
4.3 Relevant Digital Signal Processing	36
4.3.1 Selection of Illuminator Signal	37
4.3.2 Sampling Rate and Bandwidth	37
4.3.3 Method for Testing and Comparing LimeSDR and RTL-SDR	38
5 Results and Discussion	39
5.1 Testbed Verification	39
5.1.1 SDR Module Verification	39
5.1.2 RPi5 and NVME Testing	42
5.1.3 Antenna Testing	42
5.1.4 GPIO and Software Executable Testing	42
5.1.5 Detection Edge Processing Comparison	43
5.1.6 Enclosure Creation	44
5.2 RTL-SDR vs LimeSDR Detection Comparison	45
5.3 Overall Design Cost	47
5.4 Comparison to Existing Work	48
6 Conclusion	50
6.1 Summary	50
6.2 Limitations	50
6.3 Possible Future Work	51
7 Bibliography	52
Appendices	56
A Code and Results	57
A.1 GitHub Repository	57
A.2 Youtube Channel with Demonstration	57
B System Initialization and Testing	58
B.1 SoapySDRUtil LimeSDR Probe Output	58
B.2 SoapySDRUtil RTL-SDR Probe Output	62
B.3 Crontab Configuration	63

List of Figures

2.1	Monostatic (a) and bistatic (b) radar topologies [32]	10
2.2	Bistatic radar geometry [22]	12
2.3	Australian radio frequency spectrum allocation HF to UHF [4]	13
2.4	Ambiguity Function of AM Signal [44]	14
2.5	Ambiguity Function of DRM Signal [44]	14
2.6	Geometry and ambiguity function [22]	16
2.7	Example of range doppler map for WiFi PBR [22]	17
2.8	Block diagram of SDR transceiver [19]	18
2.9	Correlation and FFT for Range Doppler Mapping [32]	20
2.10	Clutter suppression (lack of) in range doppler map, taken from testing area with no target	21
3.1	Comparison Table - Analog vs Digital Signals [32]	25
3.2	Hardware Compute Comparison with Real Tiem Reference [32]	26
3.3	RDM of target moving away from receiver [24]	26
3.4	Silent Sentry Passive Radar [11]	27
4.1	RTL-SDR with Simple SMA Antenna	28
4.2	RTL-SDR Block Diagram [6]	29
4.3	LimeSDR-USB Version 1.4 PCB [33]	30
4.4	LimeSDR Block Diagram [33]	30
4.5	Raspberry Pi 5 with NVME SSD [35]	31
4.6	Geometry of Over the Shoulder Antenna Placement	33
4.7	LimeSDR Software API Block Diagram	35
4.8	Digital Signal Processing Chain	36
5.1	RTL-SDR Waterfall Plot (DAB Multiplex 9A)	39
5.2	LimeSDR PSD Plot (DAB Multiplex 9A)	41
5.3	LimeSDR Waterfall Plot (Channel 7 DVB-T Multiplex 177.5MHz)	41
5.4	Antenna and Testbed Testing Geometry	43
5.5	Processing Time Comparison	44
5.6	Enclosure Design	44
5.7	QF936 Flight Path [18]	45
5.8	FFT Method Range Doppler Output: Frequency Bin Step Size Comparison	46
5.9	LimeSDR Medium Gain Range Doppler Output: Noisy Clutter	46
5.10	LimeSDR DAB High Gain Range Doppler Output: Noisy Clutter	47
5.11	LimeSDR Medium Gain Range Doppler DVB-T	47
5.12	Final Testbed	48

List of Tables

2.1	Properties of Potential IoO's	15
2.2	Comparison of SDR's [40]	18
2.3	Comparison of Single Board Computers [47]	22
5.1	Disk Read Performance: NVMe vs MicroSD Card	42
5.2	Noise Floor and SNR Comparison with -14.2 dB Gain (RTL-SDR)	42

Chapter 1

Introduction

To Do:

This section will contain a clear definition of the thesis topic, goals, project scope, and relevance of the project.

1.1 Topic and Relevance

Passive radar detection technology is a class of radar detection whereby the radar system does not emit any radiation. Instead, it uses existing electromagnetic signals in the environment, such as television or radio broadcasts, to detect and track objects. Passive radar can be bistatic, whereby the transmitter and receiver are separate, or multistatic, where there are multiple receivers. The technology has been around since the early 20th century, but has only recently become feasible due to advances in digital signal processing and computing [21]. The technology has a number of advantages over traditional radar systems. It is covert, as it does not emit any radiation, and is therefore difficult to detect and directly jam, leading to a concentrated interest from defence circles [24]. It is also relatively cheap, as it does not require a dedicated transmitter and hence has less energy consumption. Conversely, it has a number of disadvantages, such as a lower signal-to-noise ratio, and a requirement for a relatively large amount of computational power to process the received signals [21].

Bistatic passive radar detection has a wide range of applications centered around situational awareness, including air traffic control, border security, and environmental monitoring. Embedding the passive radar technology is a relatively new field buoyed by recent and increasing developments in computational power on Internet of Things (IoT) devices [32]. Key components and processes of a passive radar RX system include the antenna, the receiver hardware (software defined radio), signal sampling hardware and memory, along with the compute to complete the digital signal processing [22]. Advantages of implementing some or even all of these components in a low cost manner include increased scalability, portability, and lower reliance on external high cost hardware such as a PC.

1.2 Aims and Objectives

To explore the feasibility of a low cost embedded passive bistatic radar detection, and provide a scalable proof of concept, this thesis aims to provide a user friendly testbed for digital signal based passive radar detection. The work conducted in this thesis and the eventual prototype hopes to decrease the barriers to entry for passive radar detection technology, and provide

a platform for further research and development in the field. At a high level, the primary objectives of this thesis project are;

1. Develop an understanding and proof of concept of passive radar detection algorithms on low cost single board computers (SBC) connected to software defined radio (SDR) hardware.
2. Design and implement a small-sized modular passive radar detection system on single board computer hardware with an emphasis on user friendliness and scalability.
3. Verify the functionality of the low cost embedded passive radar detection system in a controlled environment against higher power computing results, compare the efficacy of different SDR modules and investigate the potential for scaling up to a multistatic system through a network.

1.3 Scope

This thesis focuses on the development of a hardware testbed based on software defined radio (SDR) and single board computer (SBC) technology. The scope of this thesis project is limited to the following:

- The development of a passive radar detection system using existing digital broadcast signals as illuminators of opportunity,
- The design of a small scale, modular, low cost system using single board computer hardware, specifically with simple user buttons to commence and cease data collection and processing, and
- The verification of the passive radar detection system performance and latency in a controlled environment against higher cost PC hardware.
- Exploring the potential for scaling up the system to a multistatic, remote RX system through a network.

Given that passive radar based detection is a broad topic with much academic progress and commercial technological development, this thesis will not aim to cover the broad subject area. Consequently, the following topics are out of scope for this project:

- The development of a complete bistatic passive radar detection system optimized for low latency, and object classification,
- The development of a full multistatic passive radar detection system, whereby angle of approach and precise location of a target can be determined, and
- The development of a passive radar detection system using non-digital broadcast signals as illuminators of opportunity.
- The modification and development of digital signal processing / detection algorithms optimized for latency and customised hardware applications.

Chapter 2

Background

This chapter collates the necessary background information for the project, including the fundamentals of passive radar, the use of illuminators of opportunity, range doppler mapping, radio hardware, digital signal processing, IoT architecture, and networking with embedded hardware.

2.1 Passive Radar Fundamentals

The key and unique feature of passive radar is its utilisation of existing illuminators of opportunity, such as television or radio broadcasts, to detect and track objects. The technology has been around since the early 20th century, with modern interest accelerated due to the use of passive radar systems on UHF TV signals and VHF FM radio transmission systems in the 1980's [22]. Equivalent terms used to describe passive radar include passive coherent location (PCL), and passive covert radar (PCR), parasitic radar, piggyback radar. Specifically, *bistatic* radar refers to the distributed design of the transmitter and receiver, as opposed to classic *monostatic* radar. As reflected by Figure 2.1 below, the turning parabolic of monostatic radar is able to receive both range and bearing of the signal echo, whereas passive bistatic radar measures time delay of the echos from the target, allowing doppler shift from the relative speed of the target to be measured.

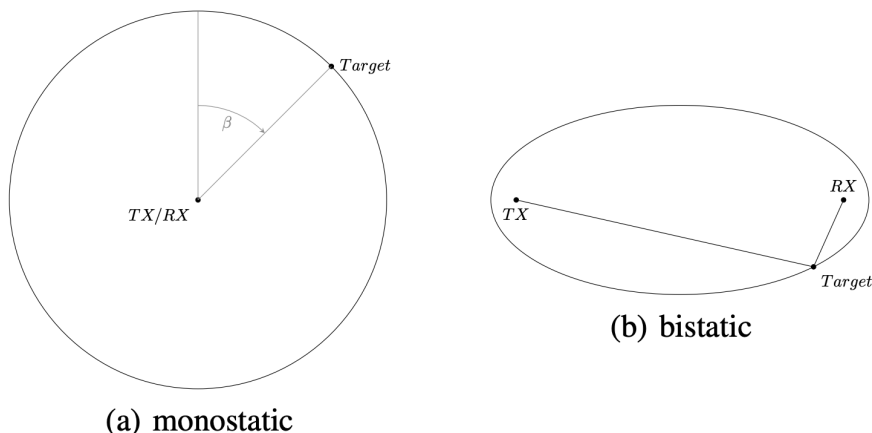


Figure 2.1: Monostatic (a) and bistatic (b) radar topologies [32]

The geometry of passive bistatic radar can be further explored and equations can be mapped

accordingly, with the distance between the transmitter and receiver R being determined by known quantities such as the baseline as reflected below in Figure 2.2.

The bistatic range R_R is given by:

$$R_R = \frac{(R_T + R_R)^2 - L^2}{2(R_T + R_R + L \sin \theta_R)} \quad (2.1)$$

The Doppler shift f_D is given by the rate of change of the bistatic range sum:

$$f_D = \frac{1}{\lambda} \frac{d}{dt}(R_T + R_R) \rightarrow f_D = \frac{2v}{\lambda} \cos \delta \cos(\frac{\beta}{2}) \quad (2.2)$$

In the case of this project, both the TX (illuminator of opportunity) and the RX (embedded passive detection system) will be static, and the target will be moving, simplifying the mathematical calculations as much as possible, resulting in the cos version of equation 2 above.

The Doppler shift will be used to determine the speed of the target as well as its relative directional motion, and the range will be used to determine the distance of the target from the receiver. Another important feature of bistatic passive radar systems is its performance which can be equated through the bistatic radar equation, which is equivalently derived as the monostatic radar equation [22].

$$\frac{P_r}{P_n} = \frac{P_t G_t}{4\pi R_T^2} \cdot \sigma_B \cdot \frac{1}{4\pi R_R^2} \cdot \frac{G_r \lambda^2}{4\pi} \cdot \frac{1}{kT_0 BF} \quad (2.3)$$

Where:

- P_r is the received target echo power.
- P_n is the receiver noise power.
- P_t is the transmit power.
- G_t is the transmit antenna gain.
- R_T is the transmitter-to-target range.
- σ_B is the target bistatic radar cross section.
- R_R is the target-to-receiver range.
- G_r is the receive antenna gain.
- λ is the signal wavelength.
- k is Boltzmann's constant (1.38×10^{-23} JK $^{-1}$).
- T_0 is the noise reference temperature.
- B is the receiver effective bandwidth.
- F is the receiver effective noise figure.

The denominator of the bistatic radar equation includes the term $\frac{1}{R_T^2 R_R^2}$. This term implies that with omnidirectional antenna patterns, the contours of constant signal-to-noise ratio (SNR) are described by the equation $R_T R_R = \text{constant}$, which represents Ovals of Cassini. These ovals represent the locations in a given PBR co-ordinate system where the distances from the target to the transmitter and receiver remain the same. In the case of directional antennas, these contours are altered. Moreover, the signal-to-noise ratio is minimized when the target is equidistant from the transmitter and receiver ($R_T = R_R$), and maximized when the target is closer to either the transmitter or receiver [22].

NEED TO MENTION / RESEARCH THE EFFECT OF NOISE AND DECIBELS EXPECTED HERE.

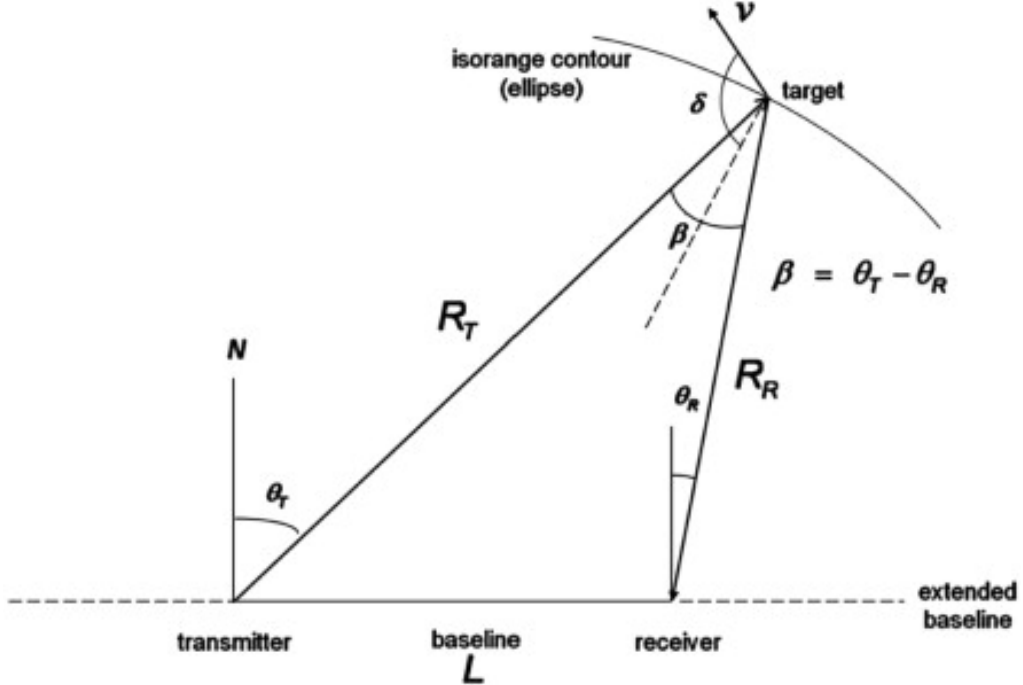


Figure 2.2: Bistatic radar geometry [22]

2.2 Illuminators of Opportunity

The illuminator of opportunity is the signal that is used to illuminate the target, and is the primary source of the signal that is received by the passive radar system. The illuminator of opportunity can be any signal that is transmitted through the air, such as television radio or even satellite broadcasts, and can be tailored to the specific requirements of the passive radar system. Firstly it is necessary to comprehend the relevant radio frequency spectrum, followed by relevant metrics for passive radar, along with the advantages of digital signals.

2.2.1 Radar and the Radio Frequency Spectrum

All wireless digital and analog signals are transmitted via a carrier frequency occupying some portion of the radio frequency spectrum. Each country regulates the use of the radio frequency spectrum, and the Australian Communications and Media Authority (ACMA) is responsible for regulating the radio frequency spectrum in Australia. The radio frequency spectrum is divided into bands, each with a specific range of frequencies, and each band is allocated for a specific use, such as television, radio, or emergency communications. The spectrum allocation chart for Australia is shown in Figure 2.3 below. In general, radar systems are capable of operating across the entire radio frequency spectrum, with the specific frequency band chosen depending on the application and the desired range and resolution of the radar system. For example, Lockheed Martin have products suited to Low Band (VHF / UHF - 30-2Ghz) which is effective for long range detection, the midband (S/C - 2-8GHZ) and the high band which is not optimal for range but resolution [28]. The below chart shows the Australian HF to UHF, with red reflecting potential illuminator signals.

In the context of passive radar, the above three bands are relevant, firstly, due to the sheer volume of broadcast signals across the HF and VHF, representing a continuous source of illumination. Moreover, most of these signals have relatively high transmit power (with transmitters geolocated to facilitate maximum coverage for a given area), enabling clear reflections

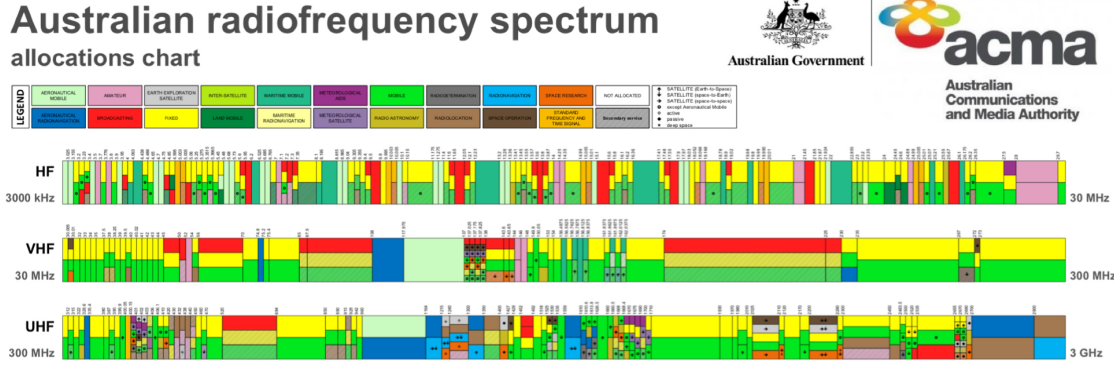


Figure 2.3: Australian radio frequency spectrum allocation HF to UHF [4]

from targets [24].

2.2.2 Key Parameters for Illuminators of Opportunity

Griffiths and Baker outline the three key parameters when selecting an illuminator [21]:

1. The **Power Density** at the target: It refers to the strength of the signal (in Watts per square meter) that reaches the target area from the illuminator. Higher power density can improve detection performance due to a stronger return signal.
2. The **Nature of the Waveform**: This includes the waveform's properties, such as bandwidth and modulation, which can affect the radar's resolution and ability to distinguish between targets and clutter. The nature of the waveform can also be impacted by the program contents of the illuminator signal, for example, the waveform of FM broadcasts is noticeably different if the broadcast is music or speech.
3. The **Coverage**: The spatial area over which the illuminator's signal is spread. Adequate coverage is essential to ensure the target is within the illuminator's effective range. As mentioned above, public broadcast signals are often optimized for a given locality.

2.2.3 Utility of Digital Illuminators

In general, digital signals are favourable for passive radar due to their large bandwidth, constant envelope and relatively large and stable transmit power. Relevant Australian terrestrial analog signals for use in passive bistatic radar include Amplitude Modulation (AM) radio, Frequency Modulation (FM). Conversely, relevant Australian digital signals include Digital Audio Broadcasting (DAB) and Digital Video Broadcasting (DVB) [9]. With DVB-T being similar to DAB with a higher bandwidth and power, potentially resulting in more signal processing steps can be required as shown by Yin et. al [48]. The images below show the ambiguity functions of two equivalent frequency band signals, DRM (low frequency digital radio broadcast) and AM radio. The DRM signal has a much wider bandwidth, and a more constant envelope, which is advantageous for passive radar systems.

Whilst the bandwidth of both the above channels is relatively small, the ambiguity functions from Thomas et al. [44] show aforementioned parameters.

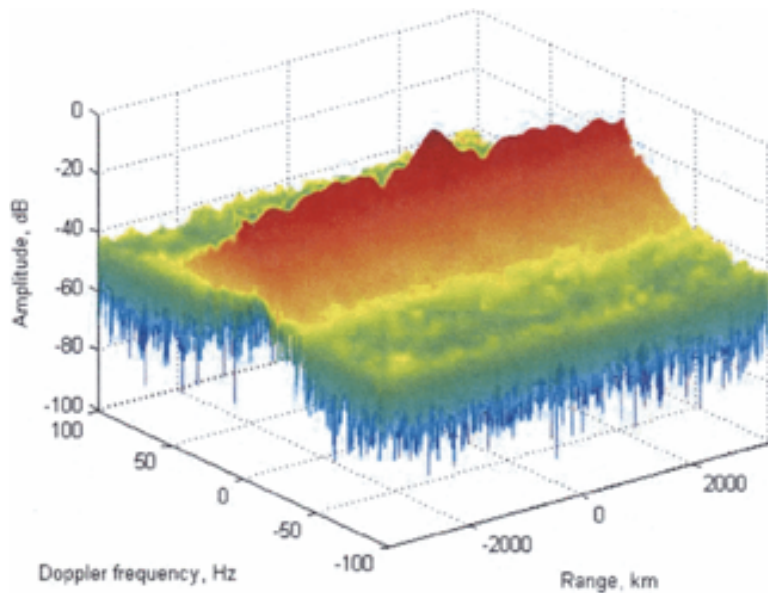


Figure 2.4: Ambiguity Function of AM Signal [44]

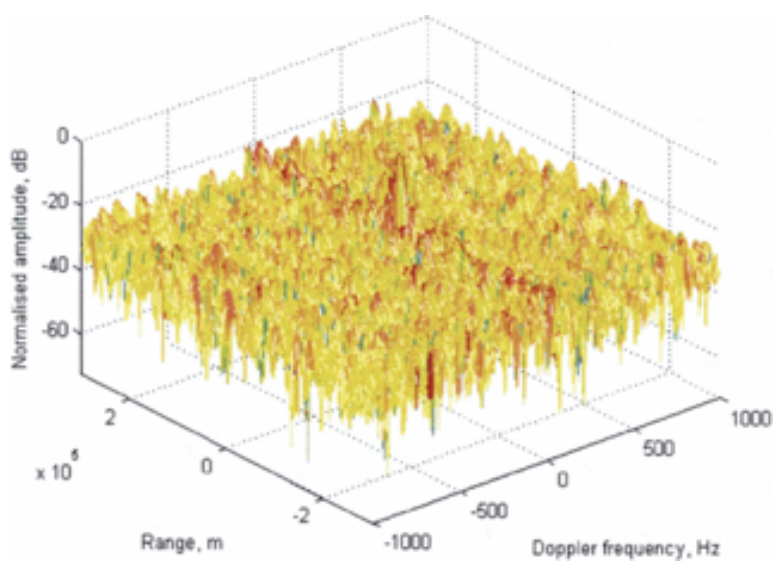


Figure 2.5: Ambiguity Function of DRM Signal [44]

Illuminator signals are not limited to terrestrial signals, they can also include signals from satellites, and can be tailored to the specific requirements of the passive radar system. Benefits of satellite based illuminators include increased coverage area, and a more evenly distributed power density [45]. An important distinction for satellite illuminators is the condition of geostationary orbit, resulting in negligible relative motion between the satellite and receiver. Another condition for satellite based illuminators is the requirement for high directional gain antennas, as the illuminator signal is transmitted from a satellite in geostationary orbit, which is approximately 35,786 km above the equator [45]. Specifically, the satellite illuminator of interest is DVB-S, digital satellite TV broadcast in the ku-band, which is a COFDM signal, with a bandwidth of 27–36MHz, and a typical power of 50–150W [7]. Notably, the large broadcast bandwidth results in significant signal processing requirements, as shown by Yin et. al [48].

Table 2.1: Properties of Potential IoO's

Broadcast network	Frequency band (MHz)	Transmitter bandwidth	Typical transmitter power (EIRP)
FM radio	88–108	0–100 kHz	10–100 kW
DAB radio	195–209	1.536 MHz	1–10 kW
DVB-T (television)	177–227	7 MHz	1–100 kW
DVB-S (satellite)	10.7–12.75(GHz)	27–36 MHz	50–150 W (transponder power)

The above table highlights some key differences in broadcast signals, potential draw backs of utilising terrestrial digital signals include geographical constraints and low signal power in rural areas, along with multipath effects in urban and high reflective areas [24].

Typical characteristics of Australian DAB+ signals include frequency of just over 200MHz, bandwidth of approximately 1.5MHz, and a minimal output power of 10kW effective radiated power (ERP), consequently covering a large area [9]. These digital signals employ a modulation scheme called COFDM (coded orthogonal frequency division multiplexing), which is a form of multi-carrier modulation that is robust against multipath interference [21]. COFDM works by dividing the signal into multiple, simultaneous streams which are orthogonal to each other, modulated at a different frequency, maximising robust signal propagation. This is particularly useful in the context of passive radar, as it allows for the target and reference signal to be received by the passive radar system even if it has been reflected off multiple surfaces, such as buildings or trees. More specifically, the Australian implementation of DAB+ is dictated by the ETSI standard EN 300 401, which specifies the modulation, coding and multiplexing of the signal [17]. DAB+ is encoded via the AAC+, with proper licensing required, the most commonly utilised forward error correction(FEC) is 3A [15]. At a high level, these protocols of DAB+ reflect a channel model which has encoding, modulation and noise handling (FEC) built in, which can be advantageous for passive radar systems. In summary, DAB along with other digital signals are advantageous for passive radar due to their wide bandwidth, constant envelope, and relatively high transmit power[23].

2.3 Range Doppler Mapping

Range doppler mapping is a technique used to determine the distance and relative velocity of targets by analyzing the frequency shift (Doppler shift) and time delay of the received signals after they are reflected off the targets. The signal response of a target at a particular range and velocity can be predicted by the ambiguity function seen in equation 2.4 [21].

$$\chi(\tau, f) = \int s_{\text{reference}}(t)s_{\text{received}}^*(t - \tau)e^{j2\pi ft} dt \quad (2.4)$$

Where:

- $\chi(\tau, f)$ is the ambiguity function.
- τ is the time delay.
- f is the Doppler frequency.
- $s_1(t)$ is the transmitted signal.
- $s_2(t)$ is the received signal.
- $s_2^*(t - \tau)$ is the complex conjugate of the received signal, time-shifted by τ .
- $e^{j2\pi ft}$ is the complex exponential representing the Doppler shift.
- The integral is taken over all time t .

The ambiguity function can be plotted, thereby visualising resolution, sidelobe patterns and any discrepancies in range and doppler. This is especially important for passive bistatic radar, whereby waveforms are not explicitly designed for radar and the geometry also has an impact [22]. Hughes visualises the geometry considerations and potential flaws of generic passive bistatic configuration below in Figure 2.6.

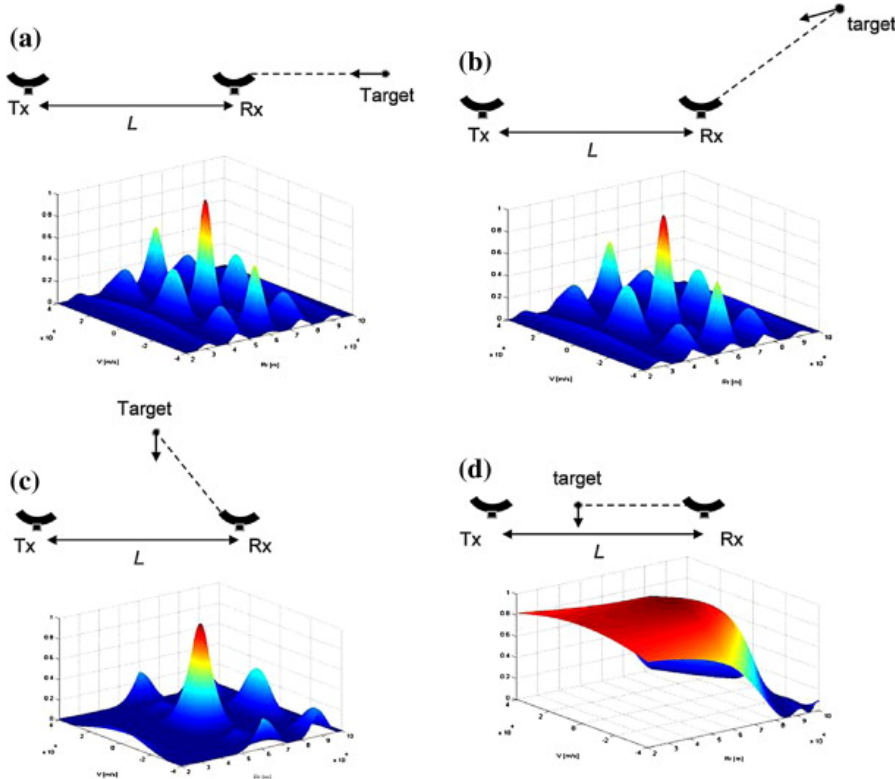


Figure 2.6: Geometry and ambiguity function [22]

Understanding the link between geometric configuration and theoretical signal properties, the practical manifestation of the ambiguity function is range doppler mapping. As shown in

Figure 2.7, the map is a heat map and is derived with filters for noise minimisation, allowing for the visualisation of the target signal with minimal clutter.

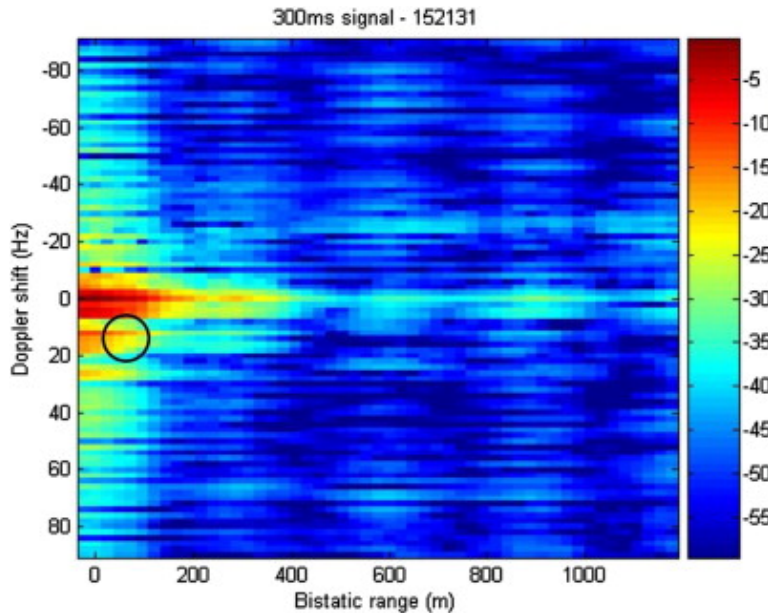


Figure 2.7: Example of range doppler map for WiFi PBR [22]

In the case of this project, the time delay will be utilised to calculate the bistatic range (x axis) and the Doppler shift will be used to calculate the relative velocity of the target (y axis). In summary, ambiguity function and subsequent range doppler mapping will be vital for mapping the DAB+ signal characteristics for given geometry and motion of the surveilled target.

MORE
DETAIL

2.4 Radio Hardware

Fundamentally, the relevant radio hardware for a passive radar project can be broken into the antenna and the SDR module. Given the low cost aims of this testbed, hardware cost and performance is a major consideration.

2.4.1 Software Defined Radio

Luckily, the proliferation of general purpose SDR hardware modules has enabled easy access to radio frequency (RF) signals [39]. In general, a SDR system can exist purely as a receiver (lower cost modules) or as a transceiver, whereby connected software (e.g. PC) are utilised for the modulation and demodulation of signals [19]. The SDR system can be used to sample the RF signal, and then process it digitally, enabling the use of a wide range of software tools for further signal processing. Typically, as seen in the block diagram below in figure 2.8, SDR's comprise of an analogue front end, an analogue to digital converter (ADC) / digital to analogue convertor (DAC), and some sort of band processing [19].

The most popular and lowest cost SDR module is the RTL-SDR, which is a USB dongle that can be used to receive (note the RTL-SDR is RX only) and decode a wide range of RF signal bands. This includes FM radio, DAB, and DVB-T signals, which are all potential illuminators of opportunity for passive radar systems. Typical bandwidth of the RTL-SDR is 2.4MHz, and the frequency range is 24MHz to 1.7GHz [38].

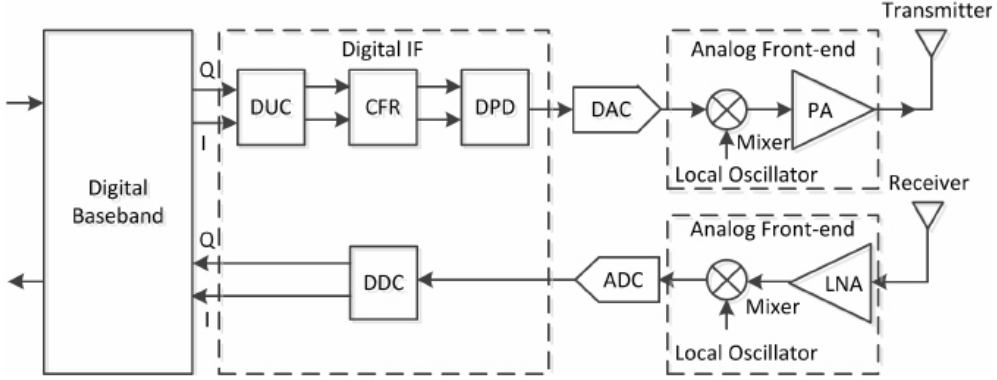


Figure 2.8: Block diagram of SDR transceiver [19]

A plethora of other SDR modules exist, with varying costs and capabilities. A range of common SDR modules are listed in the table below 2.2, along with their key specifications.

Table 2.2: Comparison of SDR's [40]

SDR	Frequency Range	Bandwidth	RX ADC	Sampling Rate
USRP	0-6 GHz	Up to 160 MHz	12-14 bits	Up to 200 MS/s
RTL-SDR	24 MHz - 1.75 GHz	Up to 2.4 MHz	8 bits	Up to 3.2 MS/s
bladeRF	47 MHz - 6 GHz	Up to 56 MHz	12 bits	Up to 61.44 MS/s
HackRF	1 MHz - 6 GHz	20 MHz	8 bits	Up to 20 MS/s
LimeSDR	0.1 MHz - 3.8 GHz	61.44 MHz	12 bits	Up to 61.44 MS/s
SDRplay	1 kHz - 2 GHz	Up to 10 MHz	12 bits	Up to 10.66 MS/s
KrakenSDR	24 MHz - 1.76 GHz	Up to 2.5 MHz	8 bits	Up to 2.56 MS/s

As performance increases for the SDR's above so does the unit cost, which is an important consideration for the testbed design explored in section 4.1. As seen in table 2.2, other than the RTL-SDR all of the SDR's have a large bandwidth making them suitable for digital illuminators, furthermore, the ADC sampling bits are often larger, resulting in more accurate signals. However, the increased resolution of an ADC also results in larger storage requirements and potentially bottlenecks in the processing chain [40]. Another interesting specification to note which is not seen on 2.2 is the number of RX channels. The RTL-SDR has one RX channel, whereas the USRP has two RX channels, which can be used to receive two signals simultaneously. This could be useful for the testbed, as it would allow for the simultaneous reception of the illuminator signal and the target signal, which could be used to improve the accuracy of the passive radar system. Specifically, the KrakenSDR features up to five channels, based on clustered RTL R820T2 tuners along with hardware to ensure the synchronisation of the channels [8]. A key advantage of the KrakenSDR in passive radar receiver systems is their ability to achieve angle of direction measurements, which can be used to determine the location of the target as shown by Cass [8].

2.4.2 Antenna

Quite simply defined by the IEEE as *That part of a transmitting or receiving system that is designed to radiate or to receive electromagnetic waves* [1], an antenna is crucial for any radio system, and in the case of passive bistatic radar, receiving all relevant signals. This section

will provide a brief background of the key concepts and types of antennas relevant to passive bistatic radar. The ITEE standard definition of terms for antennas [1] also succinctly defines the following terms which are relevant;

1. **Radiation Pattern:** This describes the angular variation in radiation at constant distances from the antenna. The radiation pattern depends on the signal strength and is categorized into three main types: Isotropic, Directional, and Omnidirectional.
2. **Directivity:** Defined as the ratio of the power density in the direction of the pattern's maximum to the average power density at the same distance from the antenna. This can be measured through front to back ratio (dB), how well can antenna block signals from the rear.
3. **Gain:** Closely related to directivity but includes losses. Gain is defined as the directivity minus any losses experienced by the antenna.
4. **Polarisation:** This refers to the nature of the electric field radiated by the antenna. If the polarisation direction is not specified, it is assumed to be in the direction of maximum gain.
5. **Bandwidth:** The range of frequencies over which the antenna operates effectively.
6. **Beamwidth:** The angle between two points on the radiation pattern where the power is at its maximum. The two main types of beamwidth are Half Power Beamwidth (HPBW) and First Null Beamwidth (FNBW).
7. **Impedance:** The ratio of voltage to current at the antenna terminals.

As with considering the SDR module, the cost versus performance trade-off is also a key factor when selecting an antenna. The most common types of antennas used in passive radar systems are the dipole antenna and the Yagi-Uda antenna. The dipole antenna is a simple, low-cost antenna that is easy to construct and has a wide bandwidth. The Yagi-Uda antenna is a more complex, directional antenna that has a higher gain and a narrower bandwidth. Given the utilisation of digital broadcast signals with relatively high power, a simple dipole antenna may be sufficient for the testbed, however, the Yagi-Uda antenna may be required for more complex applications. High gain directional antennas can be chained together to receive signals from all directions, and in a passive radar context, determine the direction of the target [8].

2.5 Digital Signal Processing

Broadly, the goal of the signal processing for general passive bistatic radar is to extract a range doppler map from a received signal. Obtaining a range doppler map involves a few steps, with specifics depending on the IOO chosen along with number of sampling channels. Furthermore, there is the option of autocorrelating these signals via correlation integrals which is the most time and compute intense, or through Batches algorithm in the frequency domain [32]. Prior to the advent of digital broadcasts, analogue broadcast processing involved comprehensive filtering and synchronisation of at least two input channels[31]. However, more recently, given the nature of DAB / DVB-T and its COFDM modulation, filtering and synchronisation can be replaced with reconstruction of the surveillance signal [5], replacing the need for dual channel configuration. Fundamentally, the single channel version of this correlation is the direct signal

(given its strength) compared with a time lagged version of itself given the refection from the target, as reflected in 2.4. Mahfoudia, et al. demonstrate the methodology behind single channel correlation and reconstruction with a DVB-T illuminator, combined with clutter suppression techniques [27]. For radar systems, as opposed to communication systems, the contents and packet structure of the signal is not necessarily relevant, rather the similarities of signals 2.4.

The simplest, yet probably most computationally intense method of processing the doppler map is via traditional FFT-based correlation. It works by correlating large portions of the signal in time and frequency domains, with doppler shifts applied, creating frequency bins which are used to correlate with the received signal in the frequency domain, thereby obtaining any doppler shift experienced by the target. As for the time domain, the range estimates of a target can be obtained by taking the inverse fast fourier transform (IFFT) of the correlated signal in the frequency domain, providing the relevant time delay (and therefore range). The process can be repeated over multiple windows of a given signal and then combined to create a range doppler map [25].

The computationally intense FFT correlation method can be refined and optimised by taking slow time 'batches', reducing the size of required FFT calculations. Once the signal has been received and windowed, according to Moser et. al, a FFT the size of 2048 for the range domain and 512 for the doppler domain can be computed [32], see Figure 2.9.

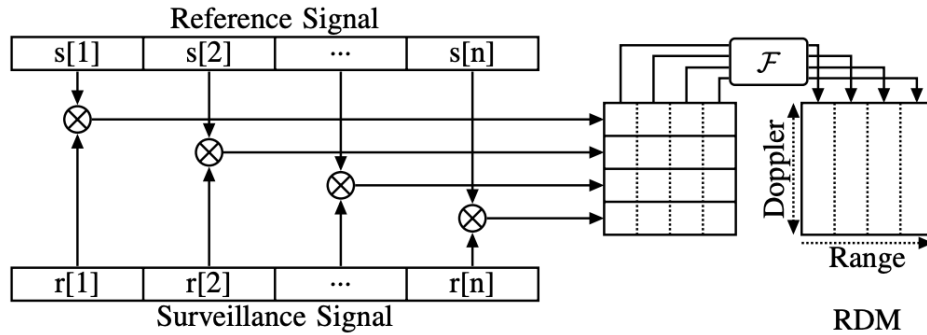


Figure 2.9: Correlation and FFT for Range Doppler Mapping [32]

Given that single channel configurations are vulnerable to noise, interference and multipath, the outputs of pure correlation can result in clutter on the range doppler map. In the case of single channel configuration for PBR, the signal from the target (already quite weak) can be obstructed by unwanted reflections from buildings, trees, and other objects [21]. The above algorithms can be combined with a decluttering chain, which can implement something along the lines of a weiner filter, or a matched filter, to remove unwanted signals from the range doppler map [22]. The implementation of clutter suppression algorithms, specifically background mean subtraction (BMS) and guard mean subtraction (GMS) has been shown by Zhang et al, working to clear up range doppler maps [49]. This clutter suppression is especially necessary around low doppler shift targets, as the clutter can be mistaken for the target signal. The presence of clutter given lack of suppression can be seen in Figure 2.10 below (yellow higher intensity pixels).

Logically, the process above reflects the most computationally intensive step of the project ... hence, considerations with regard to signal processing algorithms will need to be taken in order to keep the overall detection system low cost, despite it not being a major factor of the testbed creation itself.

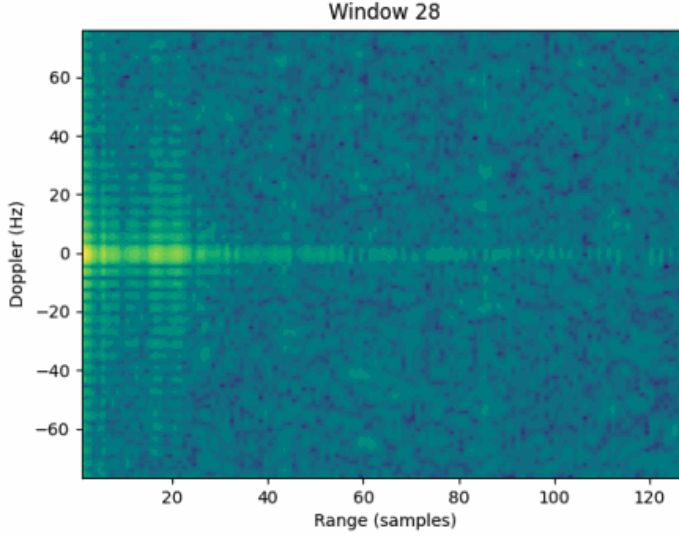


Figure 2.10: Clutter suppression (lack of) in range doppler map, taken from testing area with no target

2.6 IoT Architecture

The IoT architecture in the scope of this project refers to the computational platforms utilised to undertake the digital signal processing which then maps to tracking and detection of the target. At a high level, ITEE defines the Internet of Things (IoT) as "*as a world of interconnected things that are capable of sensing, actuating, and communicating among themselves and with the environment ... provides the ability to share information and autonomously respond to real/physical world events by triggering processes and creating services with or without direct human intervention*" [2]. In terms of PBR, existing studies have demonstrated the ability of off the shelf laptops [42], and there is a few studies that use IoT platforms for FM signal processing [32]. The vital consideration when exploring hardware are the DSP and sampling requirements for a given illuminator signal and antenna configuration. More broadly, IoT hardware has been used in a range of general tracking and detection applications. A prime example of this is the Flightradar24 service which utilises a network of ADS-B receivers to track aircraft in real time, where they provide a hardware kit of a Raspberry Pi and a DVB-T dongle (RTL-SDR) [18], channelling the data to a central server for processing and mapping.

According to Schupbach et. al [41], the broad scope capability requirements of the computational platform and associated processing can be grouped into signal acquisition, signal reconstruction and then the correlation function calculation. With a single board computer, this can be largely achieved through a combination of software libraries along with python script, however the hardware facilitating this processing is a key consideration. Largely, the IoT hardware is limited to single board computers, as microcontroller units (MCU) are not capable of the sampling and detection processing requirements, along with the fact that the project requires a full operating system for relevant SDR libraries. Exploring other potential architecture such as FPGA's, again are not as well suited, given their high cost and complexity, although there is precedent for the signal processing and recording [30]. A range of single board computers are available, and can be compared primarily based on their processing power, memory / memory access, and cost [47], as viewed in the table below.

SBC	CPU	RAM	Storage Access	OS Support	Size (mm)	Price (USD)
Raspberry Pi Zero 2 W	Quad-core Cortex-A53, 1 GHz	1GB	microSD	Raspberry Pi OS, Linux	65 x 30	15
Raspberry Pi 4	Quad-core Cortex-A72, 1.5 GHz	2/4/8GB	microSD, USB	Raspberry Pi OS, Linux	85.6 x 56.5	35-75
Raspberry Pi 5	Quad-core Cortex-A76, 2.4 GHz	8GB	microSD, PCIe (through HAT), USB	Raspberry Pi OS, Linux	85.6 x 56.5	from 60
Nvidia Jetson Nano	Quad-core Cortex-A57, 1.43 GHz	4GB	microSD, PCIe (through adapter)	Ubuntu, JetPack	100 x 80	100
Orange Pi 5	Octa-core Cortex-A76/A55, 2.0 GHz	8GB	eMMC, microSD, PCIe	Android, Linux	90 x 60	80

Table 2.3: Comparison of Single Board Computers [47]

There is precedent of previous use for the Raspberry Pi platform as demonstrated by Moser et. al [32] An alternate, higher powered choice in which Sednall demonstrated is the higher powered Nvidia Jetson, which includes faster processing times due to its quad core architecture [42]. The price for these options is \$60 compared to \$250 respectively. Ultimately, the choice of embedded IoT hardware for the project can be reduced to the trade off between low cost and processing power, and will be a key consideration in the project plan. Furthermore, there is possibility to design custom hardware or utilise the GPIO functionality of the single board computer, as reflected by the high level definition of IoT architecture by ITEE [2].

2.7 Networking with Embedded Hardware

Given that the overall goal of this thesis project is to create a low cost, embedded passive radar detection system, valuable to consider how this would be visualised, be it via wired or wireless protocol. Essentially, depending on whether the RDM is computed on the 'edge' (ie embedded device) or on a PC, the networking requirements will differ. For example, if it is only IQ sampling completed on the embedded testbed platform, only the IQ data in the form of a .bin file needs to be transferred, however, if the RDM is computed on the embedded device, the entire RDM image / gif will need to be transferred. The following options vary in complexity and context, but all facilitate the relevant transfer of data from the embedded

device to a PC for further processing or visualisation.

2.7.1 USB Drive Transfer

The most basic method of transferring data from an embedded device to a PC is via a USB drive. This method is simple and reliable, and is ideal for applications where the data transfer rate is not critical. The data is saved to a USB drive on the embedded device, and then transferred to a PC for further processing. However, it is not ideal for real-time applications, as the data transfer is limited by proximity and a manual process is required (despite large data storage capabilities).

2.7.2 SSH

Secure Shell (SSH) is a widely-used method for remotely interfacing with embedded devices and SBC's. It allows users to securely log in to a remote device over a network and issue commands as though they were operating directly on the device. This is particularly useful for headless systems, where the embedded device does not have a monitor or keyboard connected. SSH encrypts all communication, ensuring data security. Once an SSH connection is established between the Raspberry Pi and a PC, tasks such as starting data capture, configuring parameters, or transferring files can be done directly from the PC terminal [20]. Many applications use SSH for remote monitoring and control of embedded systems, as well as for viewing the UI of SBC's, for example VNC viewer.

2.7.3 Ethernet

Ethernet is one of the most common and reliable methods for data transfer between embedded systems and PCs, offering high data transfer speeds and low latency. Ethernet is a wired networking technology that forms the backbone of local area networks (LANs). It supports high-speed data transmission, typically at 100 Mbps (Fast Ethernet) or 1 Gbps (Gigabit Ethernet) [34], making it a suitable for applications that require real-time data transfer or when working with large datasets, such as IQ samples or RDM files. Ethernet uses a network cable (e.g., CAT5, CAT6) to connect devices in a LAN. It transmits data packets using the Internet Protocol (IP), allowing connected devices to communicate with one another. The data packets are routed through switches and routers, which direct the flow of traffic within the network. Ethernet is widely used in industrial automation, IoT, and other applications that require reliable and high-speed data transfer.

2.7.4 TCP Socket

A TCP (Transmission Control Protocol) socket is a software-based method for creating a reliable connection between two devices over a network. TCP ensures that all data packets are transmitted in the correct order and without loss, making it ideal for real-time data streaming applications such as radar data. In the case of this project the testbed would act as the client, initiating data transfer to the server (PC). This can be implemented over a wireless network [12].

2.7.5 Cloud Service

Another modern solution for data transfer between embedded devices and PCs is the use of cloud services. The embedded testbed can upload data to cloud storage, which can then be accessed from the MacBook Air, or vice versa. An obvious downside of this method is the reliance on an internet connection, and the potential for data security issues.

Chapter 3

Literature Review

This chapter will explore and summarise previous work on the topic of passive bistatic radar detection and associated hardware, ranging from academic literature to currently available commercial technology. The literature review will be divided into the following sections: low cost IoT hardware receiver, digital signal based illuminator of opportunity and existing commercial technology.

3.1 Low Cost IoT Hardware PBR Receiver Design

The Swiss army have conducted a very informative pilot study utilising both FM radio and DAB+ signals as illuminators of opportunity for an IoT based receiver design. Moser et. al explore the performance of a Raspberry PI 3 GPU and CPU against a quad-core intel i7 equipped PC [32]. This paper also provided a good starting point for information regarding the difference in signal processing between digital (DAB+) and analogue (FM) illuminators of opportunity, including key characteristics as seen in Figure 3.1 .

	FM	DAB
Frequency	88 - 108 MHz	174 - 230 MHz
Modulation	analogue (FM)	digital (OFDM/DQPSK)
Bandwidth	0.05 MHz	1.536 MHz
Availability	Global	Local
Network	multi-frequency	single-frequency
Content dependency	yes	no

Figure 3.1: Comparison Table - Analog vs Digital Signals [32]

Moser et. al also provide a summary of the range doppler map generation process which itself is derived from Batches algorithm [31], including valuable performance measurements which indicate the efficacy of GPU processing over CPU processing. The specific hardware utilised in Moser's paper was a Raspberry Pi v3; 1.2GHz Cortex A53 CPU along with a 400MHz VideoCore IV GPU. As of writing, the estimated cost to recreate this exact hardware (including SDR-RTL hardware) would be approximately \$100 AUD, representing a very low cost setup. Noting that hardware has also made significant advancements since the time of the paper (2019), with the Raspberry Pi v5 now available. The paper provides good hardware reference values for real-time processing limits of DAB frame computations, a key consideration area when optimizing for low cost hardware, these comparisons can be viewed below 3.2.

Overall, this conference paper provides a good starting point for understanding the hardware requirements and limitations of a low cost IoT based passive bistatic radar receiver.

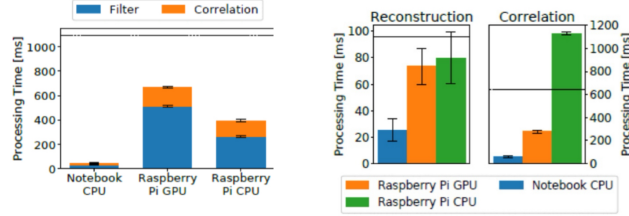


Figure 3.2: Hardware Compute Comparison with Real Tiem Reference [32]

Notably this paper is difference from the thesis proposed given that it focuses on implementing real time processing and optimisation of detection DSP algorithms on low cost hardware, rather than the design and construction of a user friendly, scaleable testbed, which also explores different SDR modules.

3.2 Illuminators of Opportunity

Throughout the literature review, a range of papers exploring illuminator signals were explored, the DTSO report Written by Palmer, Palumbo, Van Cao, and Howard provides a good theoretical basis. Whilst the scope of this proposal is confined to terrestrial illuminators (specifically digital audio), Palmer et. al highlight the wide range of use cases made available by other illuminators, including satellite signals and mobile phone signals. The report also provides a good overview of range doppler mapping, and target classification properties (despite the scope of this proposal not including target classification). Specifically, their is notable contrast of the utility of digital singals over analogue signals as demonstrated via the figures in 2.2, with the autocorrelation output of a terrestrial analogue TV broadcast shown to have poor IoO characteristics.

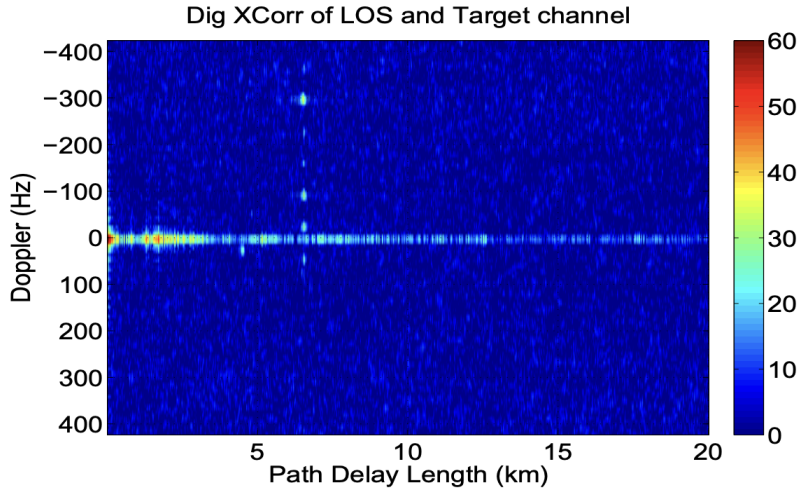


Figure 3.3: RDM of target moving away from receiver [24]

As seen above in Figure 3.3, in the .gif version of the image, the dot can be seen moving upwards (indicating motion away). This example also reflects effective de-cluttering of the RDM, a key step in passive tracking. An important consideration raised in this report is the edge case whereby the target moves along the bistatic ellipse as viewable in Figure 2.1, resulting in the doppler shift to be minimal and making tracking difficult.

Palmer et. al also effectively highlight the utility of thresholding and constant false alarm rate (CFAR) processing in the context of passive radar, with the CFAR algorithm being used to detect targets in the presence of clutter. CFAR represents a potential exploration area for this thesis in order to extend the effective detection range of a testbed via the differentiation of target and clutter signals.

3.3 Existing Commercial Technology

Commercial industry has been developing passive radar for a number of years now, with the majority of such development occurring in the military space. Specifically, these innovations are in the realm of air surveillance and can be either ground based or air based [22]. Structurally, passive radar provides numerous advantages for defence applications including covert tracking due to the lack of a transmitter.

Lockheed Martin - SilentSentry: One of the earliest commercial products utilising passive radar, the SilentSentry utilises analog illuminator signals with a dual horizontal linear phased array antenna to passively detect and track airborne targets [24]. It claims a detection range of up to 200km with an azimuth coverage of 60-360 degrees. Given the analog nature of the signals (FM and other terrestrial signals), it has a receiver for the direct line of sight signal and the echoed target signal before applying a signal processing algorithm. The silent sentry also claims capability of detecting multiple targets simultaneously, a key feature for air surveillance applications [11].



Figure 3.4: Silent Sentry Passive Radar [11]

Since the release of Silent Sentry in 1998, there have been a number of other releases from different countries, each utilising a combination of different illuminators. Notably, these systems include BAE Systems CELLDAR (UK), Thales Homelander Alerter (France), and Silentium Defence Maverick (Australia).

Chapter 4

Methodology and Design

This chapter contains the design decision and steps taken to complete the testbed creation and testing. The project can broken into the three main areas of hardware, software and digital signal processing.

4.1 Hardware

4.1.1 Software Defined Radio

The fundamental hardware aspect for this project is the Software Defined Radio (SDR), specifically, the SDR receiver module. As mentioned in section 2.4, software defined radio technology has been recently experienced decreasing costs and proliferation [39]. Broadly, the testbed was designed to accomodate a potential range of USB-A capable SDR modules, with the capability initially tested on a low cost and qualirt RTL-SDR to use as a benchmark, before progressing to later prototyping on higher end LimeSDR.

(i) RTL-SDR The low cost RTL-SDR was chosen as the initial SDR module for testbed prototyping due to its low cost and wide availability. The specifics of the RTL-SDR are stated in section 2.4, it was connected to the RPi5 and higher level M1 Mac along with a simple SMA antenna as seen in the figure below 4.1.



Figure 4.1: RTL-SDR with Simple SMA Antenna

The RTL-SDR is based on the Realtek RTL2832U chipset, and has a frequency range of 24MHz to 1.7GHz, and a bandwidth of 3.2MHz. The RTL-SDR is also relatively cheap, with a price of around \$40 AUD, coming with compatibility to a wide range of software, including

MATLAB, and GNU radio [38]. More specifically, the RTL-SDR was originally designed as a DVB-T receiver for digital TV, but due to its versatility, it has been repurposed by the hobbyist community for a wide range of RF signal reception applications. Fundamentally, the RTL-SDR is comprised of two IC chips as seen in the block diagram figure below 4.2; the RTL2832U, which is the digital TV demodulator, and the R820T, which is the tuner. The R820T is the chip that allows the RTL-SDR to tune to a wide range of frequencies, converting those signal frequencies to an intermediate baseband frequency which is processed by the RTL2832U. Inside the RTL2832U, the signal is then digitized and demodulated and sent to the host computer via USB.

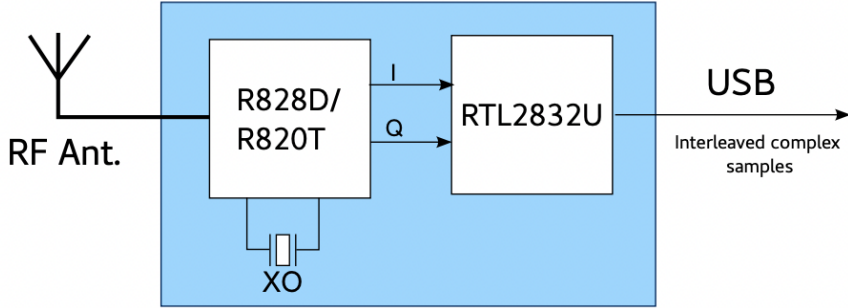


Figure 4.2: RTL-SDR Block Diagram [6]

In order to test the functionality and performance of the RTL-SDR, it was necessary to perform the following steps in isolation before integrating into the testbed, which are reflected in the results section:

- **Software Installation:** Install the RTL-SDR drivers and software on the relevant host computers (RPi5 and M1 Mac).
- **Signal Reception:** Tune the RTL-SDR to the appropriate frequency range (approx 200MHz) and receive a digital broadcast signal (with yagi-uda antenna or simple SMA monopole).
- **Signal Processing:** Process the received signal values using python to ensure the values are not junk.
- **Noise Floor Measurement:** Measure the noise floor of the received signal to account for the signal-to-noise ratio (SNR) of the system (given test location).

(ii) **LimeSDR** The LimeSDR was chosen as the higher end SDR module for the implementation and testing of the testbed. As seen in Table 2.2, the LimeSDR has a frequency range of 100kHz to 3.8GHz, and a bandwidth of 61.44MHz. The LimeSDR is also more expensive than the RTL-SDR, with a price of around \$600 AUD. Specifically, the LimeSDR used was the LimeSDR-USB Version 1.4, which can be seen in the figure below 4.3.

The actual SDR module was encased as seen in XXX 5.12, with the only relevant connections being a singular RX SMA port, power supply (6V DC) and a USB type B connection. The block diagram of the LimeSDR can be seen in the figure below 4.4, and evidently it is a more complex system than the RTL-SDR, most notably with the CycloneIV FPGA chip, which is used for signal processing and control.

In order to validate the standalone functionality of the LimeSDR, the following steps were taken, and discussed in the results section:



Figure 4.3: LimeSDR-USB Version 1.4 PCB [33]

- **Software Installation:** Install the LimeSDR drivers and software, the software required is in section 4.2.1.
- **Signal Reception:** Tune the LimeSDR to the appropriate frequency range (approx 200MHz) and receive a digital broadcast signal (with yagi-uda antenna).
- **Signal Processing:** Process the received signal values using python to ensure the values are not junk.
- **Noise Floor Measurement:** Measure the noise floor for given location.

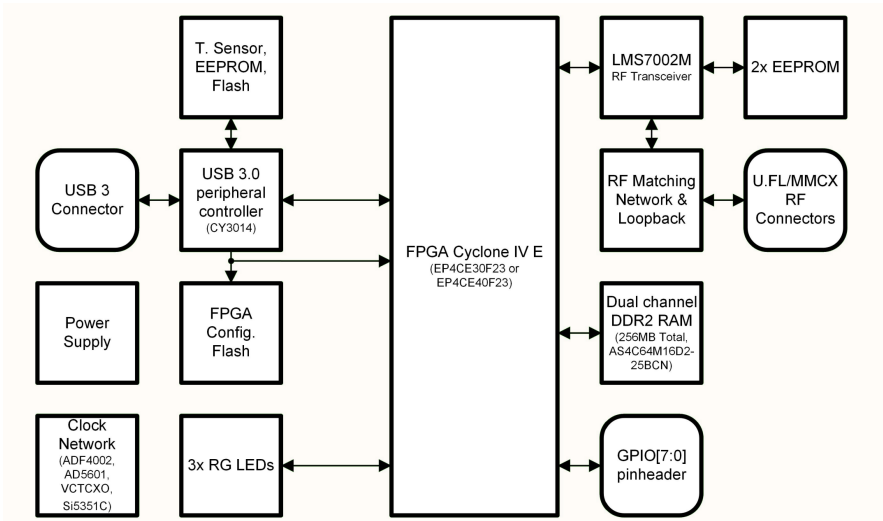


Figure 4.4: LimeSDR Block Diagram [33]

Another notable hardware feature of the LimeSDR is the LMS7002M transceiver chip which can facilitate both RX and TX capabilities, along with built in ADC/DAC (12 bit) capability [33]. The bandwidth advantage of the LimeSDR was a key factor in its selection, as the wider bandwidth allows for more data to be captured and processed, specifically in the context of the digital broadcast signal used as the illuminator of opportunity. This bandwidth advantage directly results in increased range resolution on the range doppler maps, which is a key metric for the detection of aerial vehicles. As seen in 2.2, the LimeSDR has a stated maximum sampling rate of 61.44MHz, when sampling at this rate, the bottleneck can become the USB host interface. With the maximum sample rate corresponding to about 240MB/s, which if not over USB 3.0 can limit the data transfer rate (USB 2.0 is limited to 480Mbps or 60MB/s). Moreover, as the maximum sampling rate is approached, the storage and processing requirements of the host computer also increase, becoming unreasonable at a certain point for samples of around 10 seconds.

4.1.2 Embedded Computing Platform

The embedded computing platform chosen for the testbed was the Raspberry Pi 5 (RPi5), specifically the version with 8GB of RAM [10].

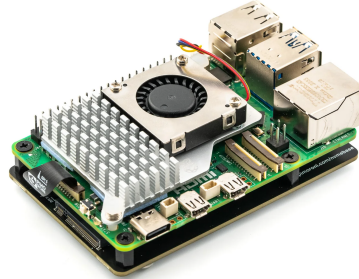


Figure 4.5: Raspberry Pi 5 with NVME SSD [35]

As seen in Table 2.3, the RPi5 has a quad-core ARM Cortex-A72 CPU, 8GB of LPDDR4-3200 SDRAM, and a 1Gbit Ethernet port. The RPi5 was chosen for its relatively low cost, small form factor, and wide range of software support. Other SBC's from Table 2.3 were considered, but the RPi5 represented the best balance of performance and cost for the project, for example, the higher cost of the Nvidia Jetson was not justified for the project requirements. The viability of the Raspberry Pi5 in the context of testbed design and functionality was analysed based on the following points:

Advantages

- **Storage:** The RPi5 supports external storage options via microSD, along with configurable HATs (hardware attached on top) for NVME SSDs, see section 4.1.3 [35].
- **Size:** Its small form factor (85.6 x 56.5 mm) - roughly the size of a credit card, makes it easy to integrate into a testbed setup. Easily obtainable cooling fan.
- **GPIO:** 40 Pin GPIO header, can be used for interfacing with a prospective testbed user. Driven by the RP1 (custom I/O controller chip) [10], the I/O is programmable with python.
- **Networking Capability:** Includes a 1Gbit Ethernet port and Wi-Fi 802.11ac, facilitating high-speed data transfer and network communication. Capable of 217.6 MB/s over Wi-Fi [34].
- **Processing Capability:** Equipped with a quad-core ARM Cortex-A72 CPU and 8GB of LPDDR4-3200 RAM, enabling 2.4 GHz clock [10].
- **Cost-Effectiveness:** Price of \$150 AUD, making it an affordable option for the project, approximately 1.5 the cost of the RPi4 (however almost double the performance) [10]
- **Software Support:** Extensive community support and availability of a wide range of software tools and libraries, especially for Linux-based systems, e.g. RTL-SDR, GNU Radio, etc. see section 4.2.1.

Disadvantages

- **Limited Built-In Storage:** The built-in storage is minimal, so additional external storage is necessary for handling large volumes of data.

- **Performance Constraints:** While powerful, it may not handle very high-frequency or complex radar signal processing as efficiently as more specialized or high-performance computing platforms, custom algorithms potentially required [32].
- **Heat Management:** Under continuous heavy load, the RPi5 may require additional cooling solutions to prevent overheating.
- **Limited I/O Bandwidth:** The available I/O bandwidth might be a bottleneck for applications requiring very high-speed data acquisition and processing.
- **Power Supply:** Requires a stable power supply of 5.1V / 15W; not ideal for potentially portable or battery-powered applications [34].

4.1.3 NVME Based Storage

Following on from the selection and testing of the Raspberry Pi 5 as the testbed computing platform, it became evident that the default 32GB microSD card used to boot and run the operating system was insufficient for the storage requirements of the project. The chosen solution for the bottleneck was to utilise a NVME SSD drive, connected via PCIe to the Raspberry Pi 5, specifically the Pimoroni Base [35]. It was necessary to test the efficacy of the NVME SSD in the context of the testbed, with the following steps take and discussed in the results section:

- **Hardware Installation:** Screw the NVME SSD drive into the Pimoroni Base, and connect the Base to the Raspberry Pi 5 via the PCIe connector.
- **Software Configuration:** Format the NVME SSD drive with operating system.
- **Performance Testing:** Test the read and write performance of the NVME SSD drive using the `hdparm` utility.

Further NVME SSD configuration details include formatting with the ext4 file system, which is the default for most Linux distributions. It was mounted to the Raspberry Pi 5 (RPi5) at the location `/mnt/nvme0n1`. The SSD connects via a PCIe x4 interface Gen 2.0, a high-speed standard commonly used for storage devices. It supports M.2 NVMe drives of the 2280 size. The specific model used is the Patriot P300 NVMe M.2 SSD with a 128GB capacity, serving both as storage and for booting the RPi5.

4.1.4 Antenna Configuration

Initially, a simple SMA whip antenna was used for the RTL-SDR, as seen in Figure 4.1. These low cost antennas are typically used for general purpose reception, and are not optimised for any specific frequency range. The whip antenna was used for initial testing and prototyping, and was capable of receiving a range of broadcast signals with a NOISE FLOOR X. Eventually a more specialised antenna was used, the Yagi-Uda antenna, which is a directional antenna that is commonly used for point-to-point communication. The Yagi-Uda antenna was used for the final testing and validation of the testbed. The Yagi-Uda was utilised with a CLF200 50 Ohm coaxial cable, which was connected to the RTL-SDR. Specifically, the 18 element UHF yagi-uda antenna, was quoted as having 15.5dB forward gain and 25dBi front-to-back ratio [14]. Typically, with directional antennas, such as the Yagi-Uda, when the gain is increased, the beamwidth is decreased, which is ideal for the testbed setup, as the antenna was placed in a specific location to receive the illuminator signal.

The physical setup of these antennas for testing comprised of an "Over the Shoulder" geometry whereby the antenna was placed behind a building in the line of sight of the TX signal (in this case Mt Cootha). For a single channel / antenna PBR setup, this geometry works to attenuate the direct path signal, and allow for the reflection to be better received by the antenna. The resulting attenuation of the direct signal from the geometry can be estimated around **-10dB** based on previous studies [29].

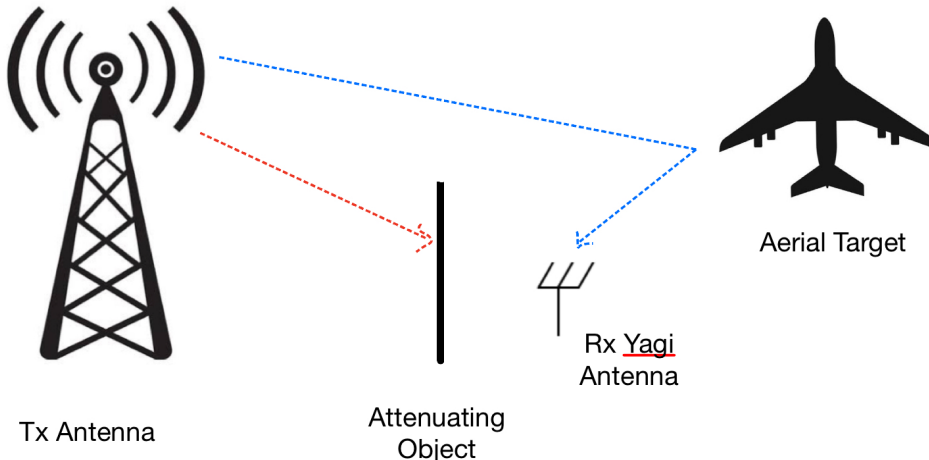


Figure 4.6: Geometry of Over the Shoulder Antenna Placement

Antenna Verification and Testing Requirements

It was necessary to have a range of hardware verification tests to ensure the antenna was functioning correctly and to quantify the signal strength of the illuminator signal. The following steps were taken to test the signal strength of the illuminator signal, and are discussed in the results section:

- **Signal Strength Measurement:** Measure the signal strength of the illuminator signal using the RTL-SDR and the SMA whip antenna.
- **Signal Strength Comparison:** Compare the signal strength of the illuminator signal using the RTL-SDR and the Yagi-Uda antenna.
- **Compare a Range of Test Locations:** Given the geography of Mt Cootha and the Brisbane air traffic flight path (INSERT RELEVANT GEOGRAPHY MAP), it was necessary to test the signal strength at a range of locations to ensure the illuminator signal was being received, and compare any contributable noise factors.

4.1.5 Testbed Design

Building off the aforementioned hardware components, it was then necessary to develop a physical testbed setup that would allow for the SDR receiver module to be connected to the embedded computing platform, and for the entire system to be powered and networked. Also, given the scope of the project, it was necessary to have a protective encasing for the Rpi5 which also implemented user functionality (ie. pushbuttons and LED's). The testbed was designed to be portable and easily deployable, with the following key components and features:

- **Enclosure:** A custom 3D printed enclosure was designed to house the RPi5, the RTL-SDR, and the NVME SSD HAT seen in 4.5. The enclosure was designed to be compact and portable, with a small form factor that could be easily transported and deployed in various environments. The enclosure was designed to be easily opened and closed, with a removable top panel that allowed for easy access to the internal components. The printed acrylic was also designed for cooling purposes, with ventilation holes on the top and sides of the enclosure to allow for airflow, bolstered by the RPi5 active cooling fan and heatsink. The model from Rasmussen was identified as a base model, with potential for appropriate modification [37].
- **User Interface:** It was envisaged that the testbed have some sort of capability that would enable physical triggering of PBR sampling and processing. Arcade style push-buttons with LED's were selected to facilitate this interface [3]. It was envisaged that one pushbutton be responsible for signal sampling and the other a trigger for embedded edge processing.
- **Power Supply:** A 5V / 15W power supply was used to power the RPi5, with a USB-C connector that allowed for easy connection to the RPi5.
- **Networking:** The ethernet port on the RPi5 was left unobstructed by the case for potential wired networking. With the main focus of being geared towards Wi-Fi based networking which was all facilitated by the RPi5 system on chip.
- **Radio Front End:** It was intended for the SDR module to be connected via the USB 3.0 port with the enclosure not designed to house the SDR unit (for versatility). Per SDR functionality, the antenna was connected via coaxial cable, also not housed in the enclosure.

In summary, the testbed was designed to be a portable, easily deployable system that could be used to test and validate the passive radar detection system. The enclosure was designed to house the RPi5, the NVME HAT, with the remaining system hardware components not specific to the testbed itself (possible to change out). This part of the project design was important for achieving the primary objectives, notably objective 2 as stated in 1.2. Details of the actual build process and testing of the enclosure are discussed in 5.1.6.

4.2 Software

4.2.1 SDR Software

When utilising SDR modules, it is necessary to have capabilities to perform necessary processing on the sampled data. This is typically done using SDR 'driver' software, which is a type of software that allows for the reception and baseband processing of radio signals using SDR hardware (ie. setting the tuner to a given frequency). Both the SDR modules utilised communicated with the host computer via USB 3.0, and utilise the libusb library for this. In the case of the selected hardware for this project, it was necessary to utilise relevant driver API's to interface with the RTL-SDR and LimeSDR, both from the testbed and the higher level M1 Mac, as shown below.

- (i) **RTL-SDR** Given the widespread use of RTL-SDR dongles, there is a range of useable software stacks and drivers available. The interface software utilised for testing and visualising

the RTL-SDR efficacy was GQRX, which is a software defined radio receiver powered by GNU Radio and the Qt GUI toolkit. GQRX is easy to use and provides a range of features for signal processing and analysis [43]. The software was installed on the RPi5 and the M1 Mac, and was used to receive and process the digital broadcast signal, also helping test the antenna. Whilst GQRX is used as a front end visualisation tool, it essentially wraps the **librtlsdr** library [26], which is the actual API driver for the RTL-SDR (specifically the RTL2832U chip [46]). The librtlsdr library handles hardware communication, tuning, and data acquisition (gain, sampling, etc) [26], and consequently outputs 8-bit I/Q samples to the host computer. This library was tested on both the RPi5 and the M1 Mac, as seen in the results section.

(ii) LimeSDR The LimeSDR requires a more complex software stack than the RTL-SDR, given its higher performance and comparatively better hardware. As mentioned in section 4.1.1 and specifically seen in the LimeSDR block diagram 4.4, the LimeSDR has a custom LMS7002M transceiver chip, along with other programmable components. However, given the relatively smaller user numbers of the LimeSDR it was more difficult to interface (given lack of documentation). The following software was used to interface with the LimeSDR, the connection between these APIs can be viewed in the software block diagram below 4.7:

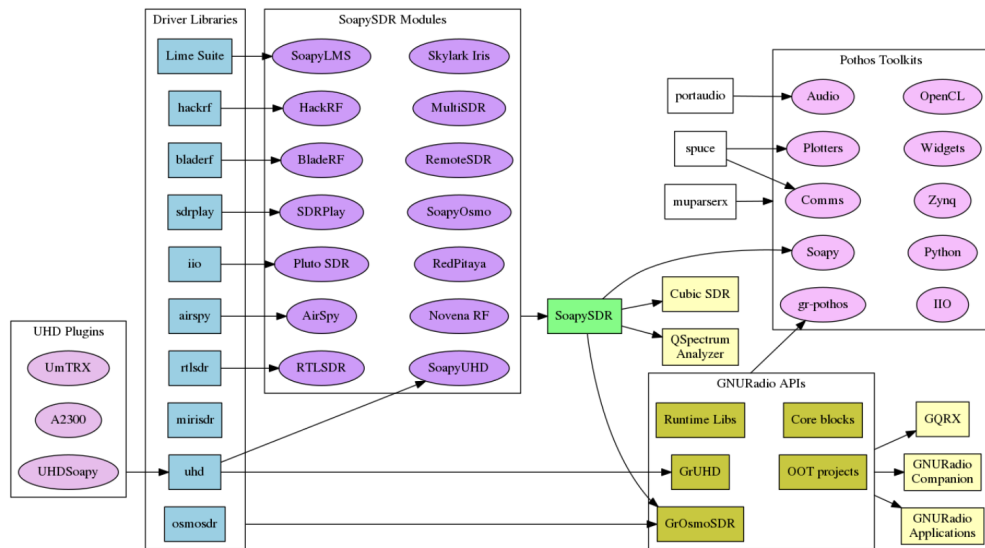


Figure 4.7: LimeSDR Software API Block Diagram

- **LimeSuite:** LimeSuite is the software that is used to interface with the LimeSDR hardware, and is used to configure the LimeSDR, set the frequency, gain, and bandwidth, and perform other functions [33].
- **SoapySDR:** SoapySDR [36] is a software abstraction layer that provides a common API for interfacing with a wide range of SDR hardware, including the LimeSDR. SoapySDR provides a simple and consistent API for interfacing with SDR hardware, and is used to communicate with the LimeSDR hardware from the host computer [?]. It essentially acts to wrap and unify the LimeSuite and LimeSDR hardware, providing a common interface for the host computer (ideal for porting from testbed to high level mac)
- **Python:** Python was used as an abstract interface, essentially calling the SoapySDR API, again, easily transferable between host computers.

In summary, the above software was selected to ensure portability between both the testbed and the higher level M1 Mac, whilst also accounting for potential SDR hardware changes. The individual component testing comprised of sampling DAB 9A, ensuring correct file parsing and basic noise floor readings.

4.2.2 Networking Requirements

Given the abundance of options explored in the background section, initially, the Raspberry Pi was connected to via SSH and VNC viewer over WiFi for configuration and testing. Eventually TCP based client-server communication was used to facilitate the transfer of data between the RPi5 and the M1 Mac. The TCP server was implemented in Python on the M1 Mac, and the TCP client was implemented in Python on the M1 Mac. The TCP client was responsible for sending the sampled data to the TCP client, which was responsible for receiving the data and processing it. This was implemented via the `socket` library in Python, and was tested on the RPi5 and the M1 Mac, with the results discussed in the results section.

4.3 Relevant Digital Signal Processing

Once the first phase of the testbed verification was completed, the next step was to implement the digital signal processing (DSP) algorithms that would be used to process the received signals and detect the presence of aerial vehicles, and then compare the results between the RTL-SDR and the LimeSDR, along with edge compute times (on the RPi5) and higher level mac processing. Whilst both SDR implementations used the same fundamental DSP algorithms (FFT and autocorrelate), there were some system factors that were impacted by the comparison. A high level overview of the processing chain can be seen in the block diagram below 4.8:

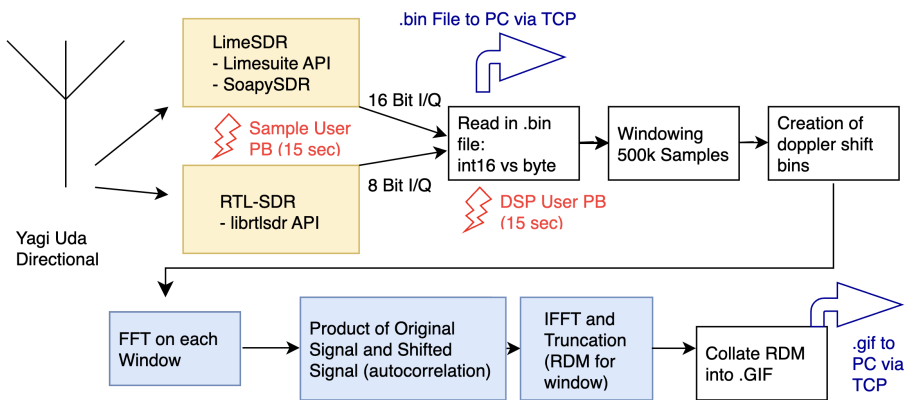


Figure 4.8: Digital Signal Processing Chain

Based on the windowing of **500k** samples, the theoretical maximum detection range of the system can be calculated. Given a default sample rate of 2.048MHz, the range resolution is calculated as follows:

$$R_{\max} = \frac{c \times N}{2 \times f_s}$$

$$R_{\max} = \frac{3 \times 10^8 \text{ m/s} \times 500,000}{2 \times 2.048 \times 10^6 \text{ Hz}}$$

$$R_{\max} \approx \frac{1.5 \times 10^{14}}{4.096 \times 10^6} \approx 36.6 \text{ km}$$

Thus, the theoretical maximum detection range is approximately 36.6 km. However, this is a theoretical maximum, and without the use of filtering and clutter suppression, the actual detection range will be much less. Furthermore, the actual detection range is also influenced by factors such as TX/RX geometry along with the other geographical factors [24]. The actual range, known as the dynamic range, is dependent on the relative position of receiver, target and transmitter as shown by Hughes in 2.2 [22].

4.3.1 Selection of Illuminator Signal

The illuminator of opportunity primarily explored for this project is the DAB+ signal, and the target signal will be aerial vehicles - most likely in the form of civilian passenger jets. The DAB+ signal is a good option due to its high power density, and its relatively high bandwidth, which can be used to improve the radar's resolution and ability to distinguish between targets and clutter. Moreover, the geographical proximity of a DAB+ transmitter at Mt Cootha to the University of Queensland, St Lucia campus, making it a potentially ideal choice for the project. Another prospective digital illuminator signal is DVB-T (digital video broadcast - terrestrial), which is similar in its digital modulation to DAB, but provides increased bandwidth and signal power [16].

4.3.2 Sampling Rate and Bandwidth

Fundamentally, the LimeSDR supports much higher sampling rates and bandwidths than the RTL-SDR, with the LimeSDR having a maximum sampling rate of 61.44MHz compared to the RTL-SDR which has a maximum sampling rate of 3.2MHz. This difference in sampling rate and bandwidth has a direct impact on the range resolution of the radar system, with the LimeSDR being able to achieve much better range resolution than the RTL-SDR. The range resolution is dictated by the sampling rate (therefore bandwidth) according to the below:

$$\Delta R = \frac{c}{2B}$$

where:

- ΔR : Range resolution (meters)
- c : Speed of light ($3 \times 10^8 \text{ m/s}$)
- B : Signal bandwidth (Hz) - DAB 1.536 MHz, DVB-T 7.5 MHz

The sampling rate and bandwidth of the SDR modules were tested and compared, with the results discussed in the results section. Based on the above equation, when sampling with a DVB-T signal / higher sampling rate the range resolution is improved, which is a key metric for the detection of aerial vehicles. The range resolution for each illuminator was:

- **DAB+ Signal:** $\Delta R = \frac{3 \times 10^8}{2 \times 1.536 \times 10^6} = 97.65625$ meters - with IQ oversampling of 2.048Mhz, the range resolution is 73.2m.
- **DVB-T Signal:** $\Delta R = \frac{3 \times 10^8}{2 \times 7.5 \times 10^6} = 20$ meters

4.3.3 Method for Testing and Comparing LimeSDR and RTL-SDR

Both SDRs were connected to the RPi5 testbed and were used to receive the same digital broadcast signal. The received signals were then processed using the same DSP algorithms, and the results were compared. The following steps were taken to test and compare the LimeSDR and RTL-SDR:

- **RTL-SDR** Utilise the RTL-SDR to sample DAB+ 9A, in the algorithm, as seen in the block diagram 4.8, the fmap step size was varied to determine the optimal range resolution.
- **LimeSDR** Centered around DAB multiplex 9A, a range of sampling frequencies were applied: 2000MHz, 4000MHz, 80000Mhz - and then also experiment with a DVB-T signal of 177.5Mhz (channel 7 Brisbane). It is assumed that the DVB-T signal will provide a better range resolution, and thus better target detection.

Chapter 5

Results and Discussion

5.1 Testbed Verification

Before the testbed was used to facilitate comparison between different SDR modules detection performance, its design and components were tested according to the steps in the methodology section. Whilst this was relatively straightforward, it was necessary to ensure the project could meet its aims of a simple, user friendly, potentially scaleable design.

5.1.1 SDR Module Verification

The RTL-SDR and LimeSDR Mini were tested to ensure they could be used in the testbed. This comprised of testing both the software driver functionality as mentioned in Section ?? and the hardware / communication functionality.

RTL-SDR The RTL-SDR was tested using a combination of librtlsdr command line tools and GQRX, both on the mac and the Rpi5. Starting with the below command to ensure the hardware was detectable:

```
rtl_test -t
```

In conjunction with the antenna testing below 5.1.3, the RTL-SDR waterfall plot was obtained via GQRX, as seen in Figure 5.1.

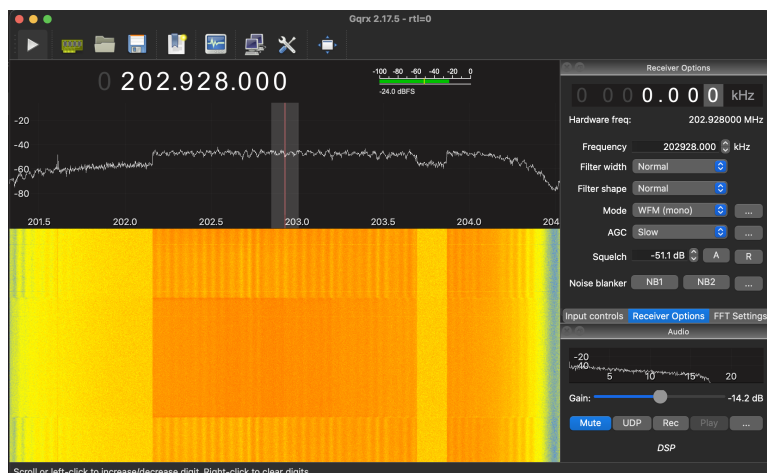


Figure 5.1: RTL-SDR Waterfall Plot (DAB Multiplex 9A)

Given that the relevant data processing was to be conducted with a python script, it was also necessary to test the ability of the RTL-SDR to sample and output data to a .bin file. This was done using the following command:

```
rtl_sdr -s 2048000 -f 202.928e6 -n 2048000 testData.bin
```

The above test was successful in saving raw IQ data to a .bin file, in the executed directory. Where the sample rate was 2.048 MS/s, the centre frequency was 202.928 MHz (DAB Multiplex 9A) and the number of samples was 2048000 (1 second of data). The *testData.bin* file size for the above example was 4.1MB, highlighting the importance of the storage medium as the sample time is scaled up, as discussed in Section 5.1.2.

LimeSDR As with the RTL-SDR, the LimeSDR hardware and software was verified, however it required more effort to test given the relative lack of driver API's. Firstly, the hardware was tested using the Limesuite Hardware API:

```
LimeUtil --find
LimeQuickTest
```

Which worked to first detect the LimeSDR and then run a series of tests to ensure the hardware was functioning correctly. Specifically the quick test verified functionality of the clock network, FPGA EEPROM, LMS7002M tuner chip, and the RF loopback. Once the physical hardware was verified it was necessary to ensure that the SoapySDR unifying API was working correctly and could detect the LimeSDR. This was done using the SoapySDRUtil command line tool and output:

```
SoapySDRUtil --find
#####
##      Soapy SDR -- the SDR abstraction library      ##
#####
Found device 0
addr = 1d50:6108
driver = lime
label = LimeSDR-USB [USB 3.0] 90706024F3821
media = USB 3.0
module = FX3
name = LimeSDR-USB
serial = 00090706024F3821
```

Further information about the LimeSDR and its channels was obtained using the following command:

```
SoapySDRUtil --probe="driver=lime"
```

The output of the above command can be viewed in the appendix B.1 and its information was used to configure the LimeSDR for sampling in the python script.

A python script was then created which utilised the SoapySDR API to sample and save data to a .bin file. The script is viewable in the Appendix ??, this was based on similar code sourced from DeepWave Digital for an Air-T SDR [13]. Noteably, as seen in the SoapySDR probe information ??, there was no automatic gain control for the LimeSDR RX1, therefore the low noise amplifier (LNA) gain was set to 30dB. The script was verified by saving a .bin file and

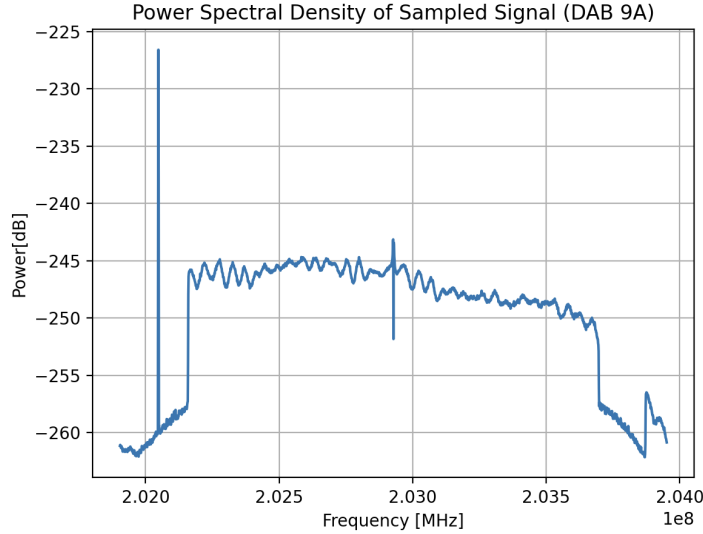


Figure 5.2: LimeSDR PSD Plot (DAB Multiplex 9A)

then plotting the PSD of the sample, showing the DAB multiplex centered around 202.928 MHz, as seen below.

Notably, given the LimeSDR has a 12 bit ADC, the output complex IQ data is 32 bits total, with a 16 bit real and 16 bit imaginary component (12 bits zero padded at LSB). The output settings of the LimeSDR are configured via the *SOAPYSDRCS16* format. This resulted in the saved .bin file being 8.2MB for 1 second of data, again showing the high storage requirements for the testbed. On the RPi5, GQRX was also able to be utilised to view the waterfall plot of the LimeSDR, as seen in Figure 5.3, adding an additional layer of verification, other than the python script and source libraries.

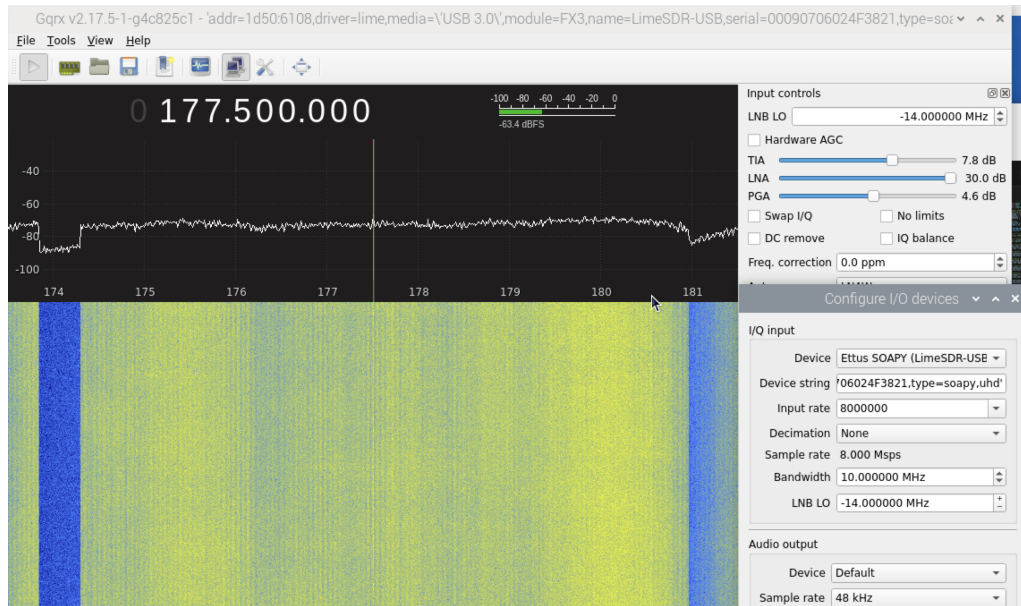


Figure 5.3: LimeSDR Waterfall Plot (Channel 7 DVB-T Multiplex 177.5MHz)

In figure 5.3, the waterfall plot shows almost 10Mhz width of spectrum bandwidth, highlighting the capability of the LimeSDR to sample a wide bandwidth of spectrum. This is in contrast to the RTL-SDR which has a maximum sample rate of 3.2MS/s, and a bandwidth of

2.4MHz. Importantly, this bandwidth and sampling rate is also variable (via source scripting or API's), and multipel different sampling rates were experimented with during testing.

5.1.2 RPi5 and NVME Testing

In order to compare and quantify the differences in the storage performance between the microSD card and the NVME SSD, a series of tests were conducted, utilising the following linux commands via the terminal of the RPi5.

```
lsblk
sudo hdparm -t --direct /dev/nvme0n1
sudo hdparm -t --direct /dev/mmcblk0
```

Resulting in the following output seen below in Table 5.1.

Table 5.1: Disk Read Performance: NVMe vs MicroSD Card

Device	Read Performance
NVMe SSD (/dev/nvme0n1)	751.22 MB/sec
MicroSD Card (/dev/mmcblk0)	84.83 MB/sec

The results in Table 5.1 clearly show the obtained significant performance increase when using the NVME SSD compared to the microSD card. Given the large amount of data that generated and processed during the SDR sampling.

5.1.3 Antenna Testing

Before calculations or detection was performed, the signal strength of the received signal was measured. This was done by first using the RTL-SDR and the monopole SMA antenna and compared to the Yagi-Uda antenna. The received signal strength, representing the illuminator DAB signal, was measured approximately 6km away from the transmitter tower. The results of the signal strength measurements are shown in Table 5.2.

Table 5.2: Noise Floor and SNR Comparison with -14.2 dB Gain (RTL-SDR)

Antenna Type	Noise Floor (dB)	Signal Strength (dB)	SNR (dB)
SMA Monopole	-60	-40.9	19.1
Yagi-Uda	-60	-17	43

The above table reflects the high gain of the Yagi-Uda antenna, which is a directional antenna, compared to the monopole SMA antenna. Overall, this testing was valuable to benchmark a noise floor and appreciate the neccessity for a high gain antenna, especially in the context of the low power target signal.

5.1.4 GPIO and Software Executable Testing

The GPIO buttons and LED's were tested using a simple python script, which was executed on the RPi5. The script was able to detect the button press and light the LED, as expected. This was a simple test, but was important to ensure the user interface was functioning correctly.

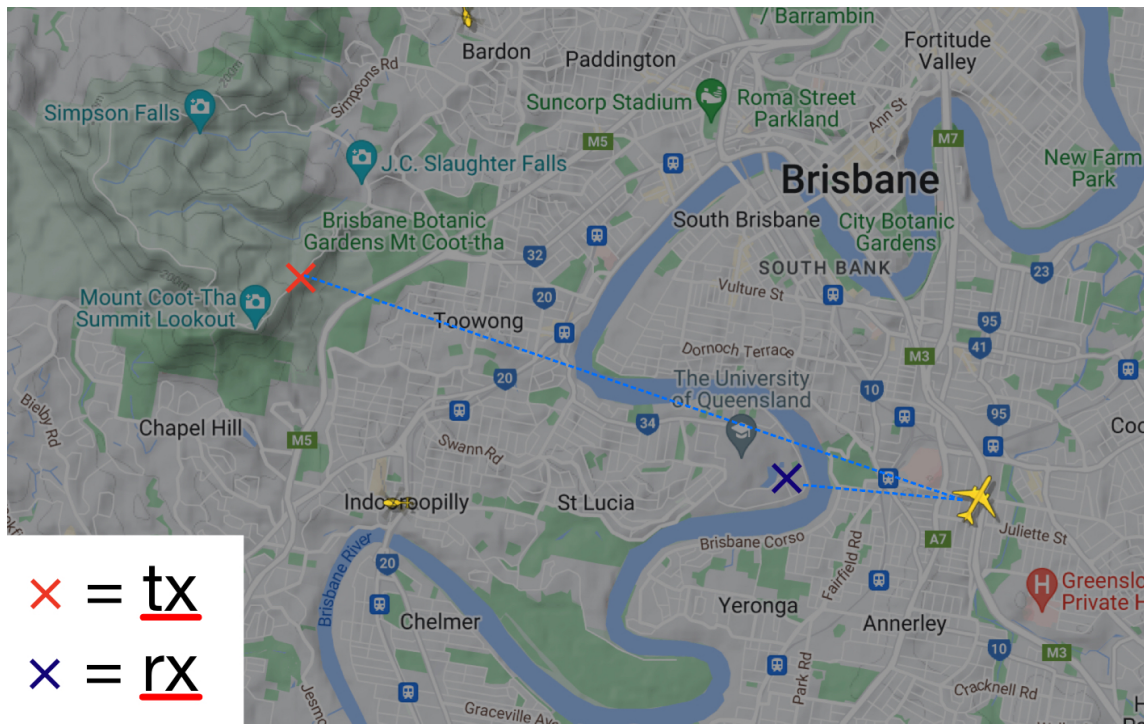


Figure 5.4: Antenna and Testbed Testing Geometry

This was implemented via the gpiod library, which was installed on the RPi5. Specifically, the script utilised the gpiochip4 which is the GPIO chip on the RPi5.

Once basic arcade button functionality had been established, using the *subprocess* library, the python script was tested executing the RTL-SDR sampling script as below:

```
rtl_sdr_process = subprocess.Popen(['rtl_sdr', '-s', '2048000', '-f',
'202.928e6', '-n', '2048000', 'testData.bin'])
```

This was tested with the lime SDR on the Debian based RPi5, and worked well. On both the RPi5, the config/sampling and processing functionality was implemented through separate Jupiter notebooks, for ease of use and debugging purposes along with timing and performance testing. These notebooks were migrated across to scripts for the final testbed implementation. The scripts were tested and integrated with the GPIO buttons and LED's, and the user interface was tested to ensure the user could start and stop the data collection and processing. In order to ensure execution at boot/run time on the RPi5, the main testbed python script was configured via a **crontab** entry, which was tested and verified, and is viewable in the appendix. The efficacy of this was tested via running the below command after boot:

```
ps -ef | grep python
```

The python script that is run by the crontab essentially polls the latch user buttons, and then sample and compute the data appropriately. The code for the python script and the crontab entry can be viewed in the appendix .

Add to
appendix

5.1.5 Detection Edge Processing Comparison

Other than some configuration changes, the processing scripts for M1 Mac and the RPi5 were essentially the same, revolving around range doppler processing windows of 500K samples.

The figure below shows the processing time for the M1 Mac and the Rpi5, with the Rpi5 taking approximately 6 times longer to process the same amount of data.

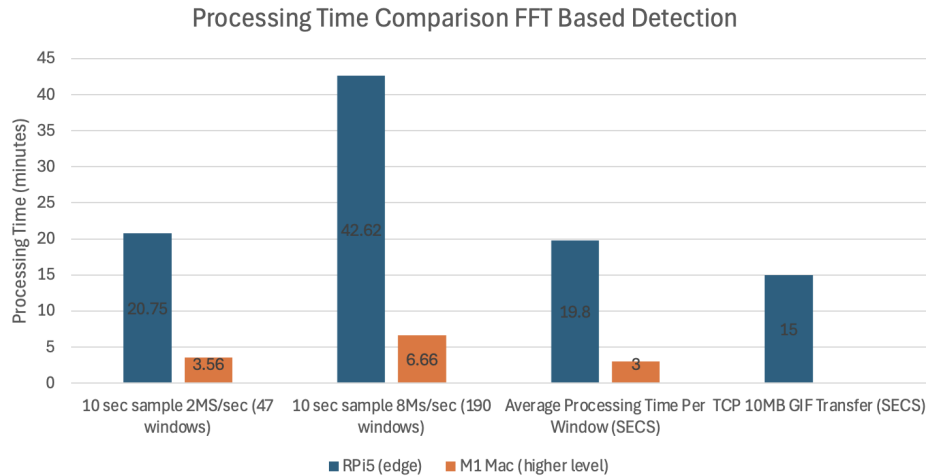


Figure 5.5: Processing Time Comparison

The difference above is as expected, given the M1 Mac has a 8 core CPU and 16GB of RAM, compared to the Rpi5 which has a 4 core CPU and 8GB of RAM. The results highlight how networking the .bin files to a more powerful computer for processing could be a potential solution to the Rpi5's processing limitations.

5.1.6 Enclosure Creation

Once the functionality of the testbed was verified, the enclosure was designed and 3D printed. The case design was modelled off source code from [37], however it was necessary to enhance the original design with cutouts for the user buttons and also stretch the top of the case to accomodate the SMA connectors and buttons.

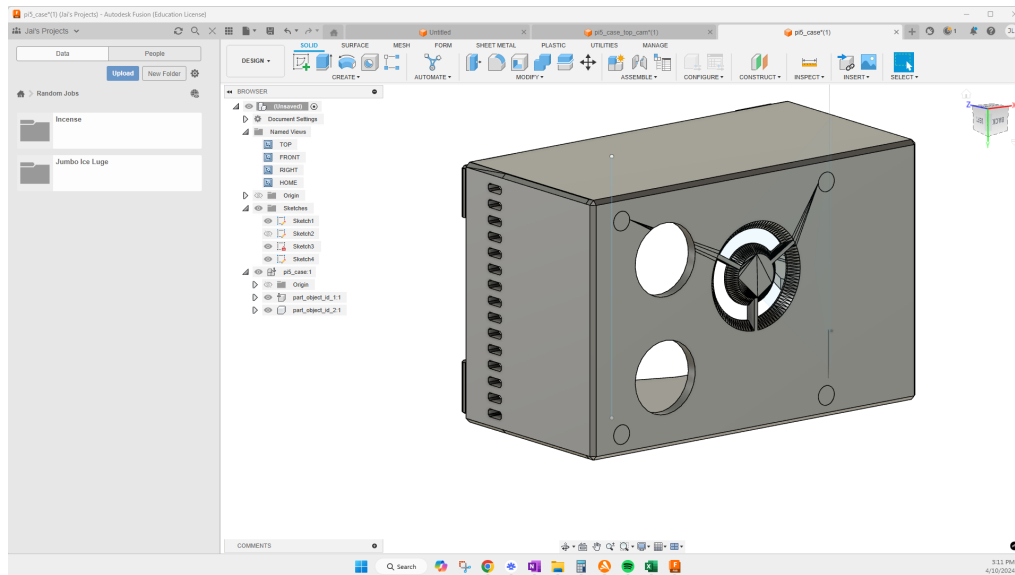


Figure 5.6: Enclosure Design

Fusion 360 was used to design the case, and the STL files were then 3D printed. The design of the final case design can be seen in Figure 5.6. The case was printed using a Bambu Lab

P1S 3D printer, utilising the default PLA filament, which is not ideal given the potential heat generated by the RPi5 and the LimeSDR. The case was printed in two parts, the top and the bottom, and then assembled. However, given the active and passive cooling requirements of the RPi5 and the LimeSDR, it was deemed fit for purpose.

5.2 RTL-SDR vs LimeSDR Detection Comparison

RTL-SDR detection was performed via the testbed first and yielded successful detection results despite lack of clutter suppression and zero doppler cancellation. LimeSDR range doppler mapping was attempted unsuccessfully due to presence of overwhelming zero doppler clutter.

RTL-SDR Detection

Firstly, the FFT algorithm was conducted on 15 seconds of RTL-SDR data, with the DAB signal at 202.928 MHz. The first specific flight was QF936, a Boeing737 on 7 October 2024. The flight path and range doppler maps are shown in Figure 5.7.

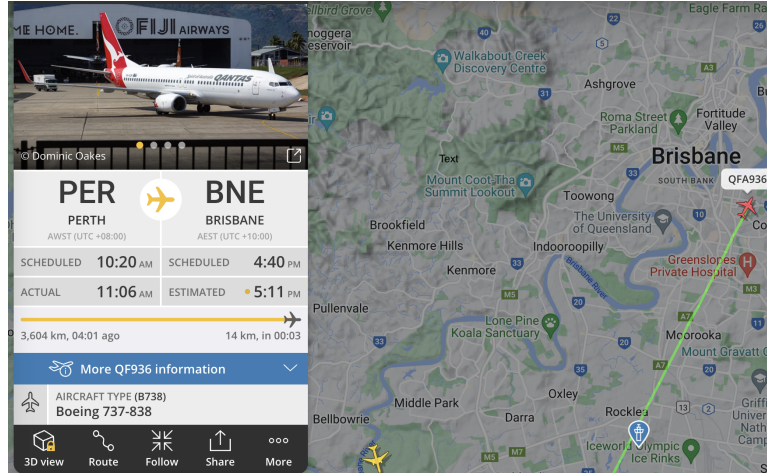


Figure 5.7: QF936 Flight Path [18]

The GIFs of the detection over the space of 97 windows, and can be viewed in further detail in the appendix A. In terms of understanding the range doppler map, detection at around the 25th sample bin reflects a detection range of approximately 1.8km, which is consistent with the flight path of QF936. Furthermore, the doppler shifts from positive (moving towards the receiver) to negative (moving away from the receiver) at around the 50th sample bin, which is consistent with the flight path of QF936. The signal was sampled as tested in Section 5.1.1, with a sample rate of 2.048 MS/s, and a centre frequency of 202.928 MHz, using the automated gain control (AGC) of the RTL-SDR.

LimeSDR Detection

In the same test location, a range of samples were taken of passing targets on the LimeSDR, starting with a sample rate of 2000Mhz, the below range doppler map was generated in Figure 5.9.

The horizontal noise bands indicate a significant amount of zero doppler clutter, which is interesting given the RTL-SDR did not have this issue. The LimeSDR was configured using

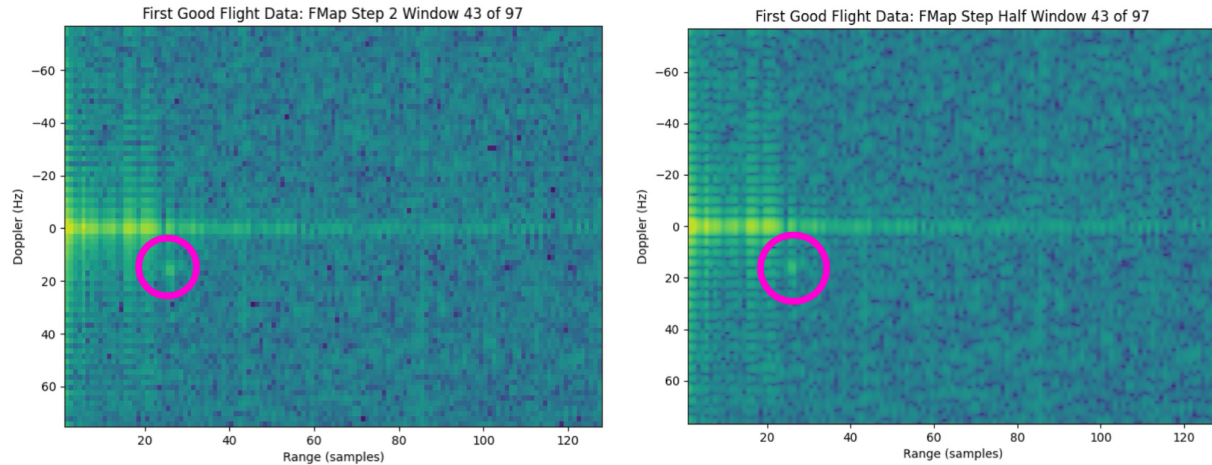


Figure 5.8: FFT Method Range Doppler Output: Frequency Bin Step Size Comparison

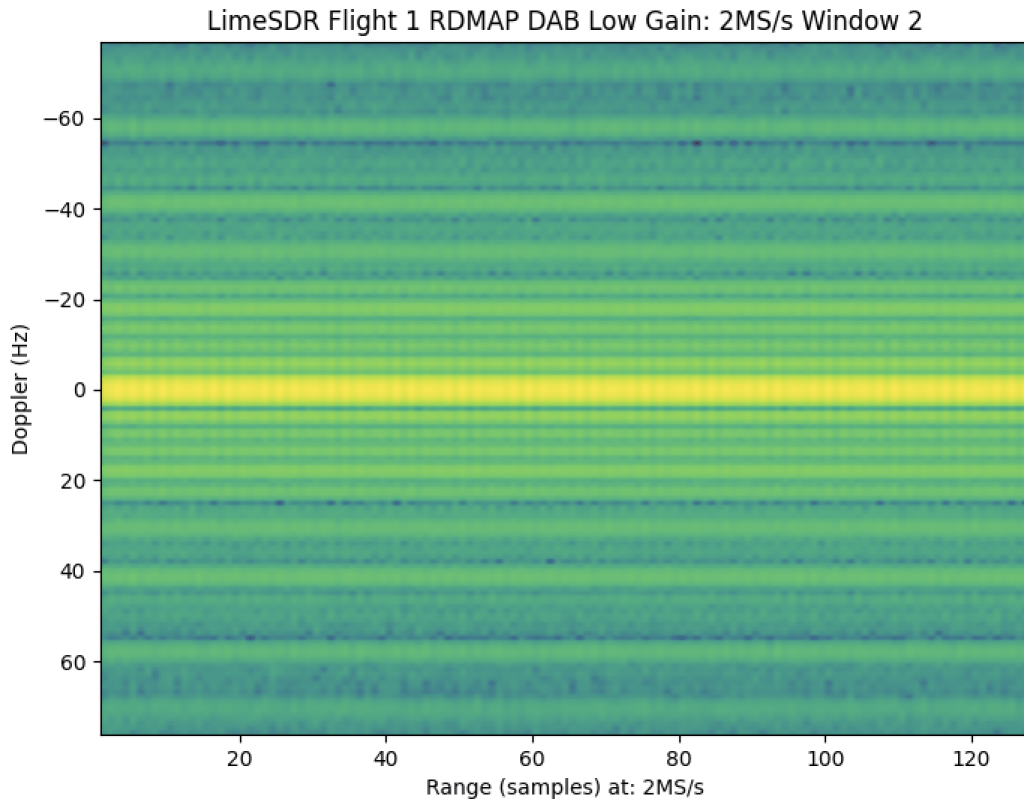


Figure 5.9: LimeSDR Medium Gain Range Doppler Output: Noisy Clutter

an LNA gain of 20dB, and a PGA gain of 5dB. The gain was increased when attempting to detect a target to no avail, with the range doppler map in Figure 5.10.

Despite being in the same location, the SNR of the LimeSDR was significantly lower than the RTL-SDR, which can potentially be attributed to the lack of AGC. A different illuminator signal was then utilised (DVB-T 177.5MHz), along with a higher sampling rate (bandwidth) of 8000Mhz, and the range doppler map in Figure 5.11 was generated.

Whilst still not being able to effectively detect passing aerial targets from the same location

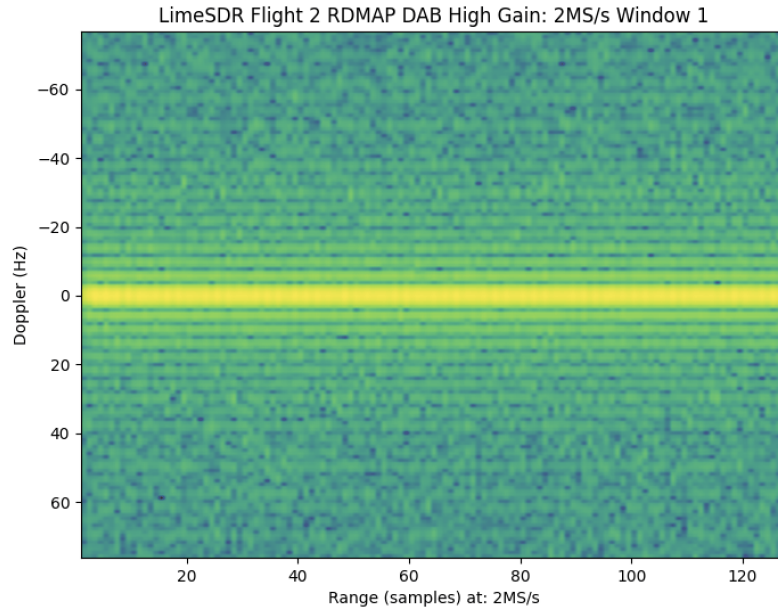


Figure 5.10: LimeSDR DAB High Gain Range Doppler Output: Noisy Clutter

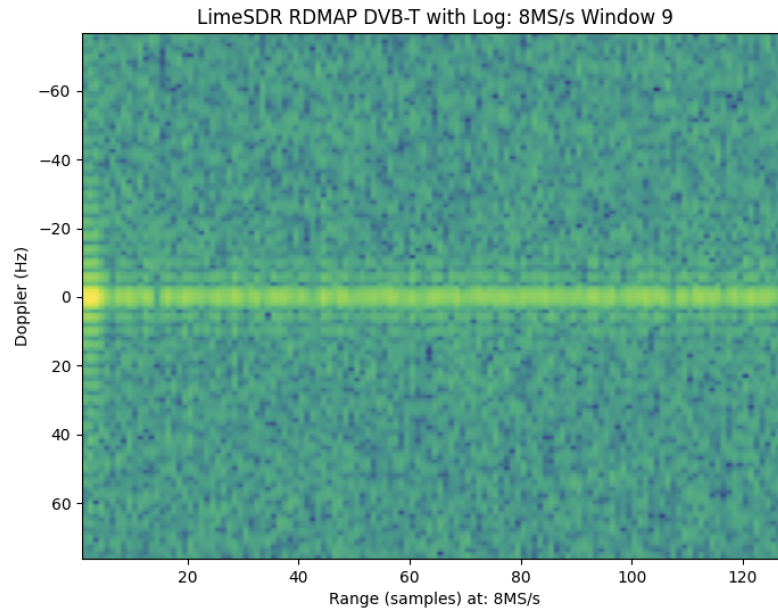


Figure 5.11: LimeSDR Medium Gain Range Doppler DVB-T

as the RTL-SDR, the generated range doppler map in Figure 5.11 shows more expected features such as clutter around the zero range as expected with autocorellation.

5.3 Overall Design Cost

The functioning test bed can broadly be broken down into the following components and their costs, with the only variance being the cost of the SDR module. The resulting cost:

- Raspberry Pi5 (8GB RAM): \$135 [10]
- Pimoroni NVME Base: \$40 [35]
- NVME Compatible SSD: \$30
- RTL-SDR: \$30 [43]
- User Buttons: \$10
- Custom Case PLA: \$5
- VHF / UHF Yagi Antenna: \$80 [14]
- LimeSDR USB 3.0 (no longer retail): \$550 AUD [33]

The image below shows the final testbed, with the LimeSDR and the RTL-SDR connected to the RPi5.



Figure 5.12: Final Testbed

This resulted in a final cost for each of the configurations:

1. RTL-SDR Configuration: \$330
2. LimeSDR Configuration: \$850

5.4 Comparison to Existing Work

To examine the implementation of the testbed along with its SDR/bandwidth comparison, it was necessary to compare it to pre-existing work. The closest work to the testbed was the work conducted by Moser et. al [32] as seen in the literature review 3.1, which utilised a Raspberry Pi 3 and an RTL-SDR to detect DAB signals. The work conducted by Moser et. al was a proof of concept, and the testbed developed in this thesis was a more user friendly, scalable version of the same concept. Analysis and comparison of these results and that of Moser et al. (the Moser study) include:

- **Hardware** Both projects utilised Raspberry Pi, with this project using the latest and updated Model. This project extended the Moser study via the addition of a higher level and cost LimeSDR. Overall, this study slightly higher in cost due to updated Pi and testbed additions such as higher speed NVME base.
- **Illuminator Signal** The Moser study explored both analogue FM along with DAB, this study focused on digital signals only, similarly with a single channel setup.
- **Signal Processing** This study did not focus on optimising already existing autocorrelation algorithms, rather demonstrating the ability to detect the signal with the RTL-SDR and LimeSDR. Moser was able to show real time detection on the RPi3 via the batch

algorithm, which based on extrapolation would be possible on the RPi5. The utilisation of a single channel configuration saved a lot of the synchronisation and matched filtering required for the FM multichannel configuration. The compute of the fourier transform correlation method was actually larger than that of Moser, wiht the Batch implementation. Interestingly, Moser provided a real time threshold value for computations, demonstrating the ability to exceed this with the RPi3 and batch algorithm, even demonstrating potential for additional CFAR processing.

- **Detection** Both studies demonstrate successful detection, however the Moser study provides a third axis on the colourless range doppler map, highlighting the signal dBFS (relative to full scale). The Moser study applied some filtering which slightly reduced noise, probably comparable to the zero range bin removal of this study.

Overall, despite differences in result comparison, noticeably the Moser study emphasising hardware compute modules, and this study looking at different SDR modules. The Moser study provided a good benchmark for the capabilities of low cost IoT hardware in PBR applications, allowing this study to further the proof of concept with modernised hardware around a similar price tag. Both show that for sub \$300 USD, a passive radar detection system can be implemented, a range of signals can be utilised, and aerial targets can quite easily be detected with minimal additional processing.

The next logical comparison is with both clutter suppression implementations and angle of arrival detection implementations. The KrakenSDR ecosystem is an example of full suite (close to) passive radar utilising five RTL-SDR tuners, with built in synchronisation. This off the shelf product (essentially a setup) comes with the preloaded open source API's preconfigured, and retails for approximately \$500usd [8].

With clutter evidently present in 5.8, another comparison can be made with the work of Zhang et. al [49], who implemented a range of clutter suppression algorithms such as BMS, GMS and CFAR. The work of Zhang et. al was able to detect smaller, further away targets, along with multiple targets in the space of one sample window.

Chapter 6

Conclusion

6.1 Summary

This thesis has explored the design and implementation of a low cost embedded passive bistatic radar detection testbed system. The testbed was built off theory and results from a range of existing studies and products aiming to provide a proof of concept for FFT based passive radar detection on low cost single board computers. The testbed was evaluated both successfully and unsuccessfully via two different SDR modules, RTL-SDR and LimeSDR, with the RTL-SDR module providing the best results. The detection processing time frames of the testbed were also compared against a high power PC. While the design of this thesis is not a complete passive radar detection system with angle of arrival and real time processing, it provides a solid foundation for future extrapolation and development.

The design has also demonstrated the proliferation and feasibility of low cost embedded passive radar detection systems, with the cost totalling at approximately \$330 AUD, along with a focus of usability and simple design. This is reflective of a higher level trend of increasing compute and decreasing cost of associated technologies ranging from SBC to SDR hardware.

6.2 Limitations

Across the design and implementation of the passive bistatic radar testbed, there were some inherent and applied limitations to the design and research conducted, summarised in the following points:

- Given the selection of a single channel antenna configuration, any potential test location required blocking of direct line of sight to IoO transmitter 4.6, in order to prevent direct signal interference.
- The use of a single RX channel also limited the potential for multistatic detection, with the testbed only capable of bistatic detection, subsequently limiting the potential for angle of arrival detection.
- Due to inherently low target signal to noise ratio and lack of extensive clutter suppression, the testbed was limited to detecting only large, relatively near targets. As opposed to extensive functionality such as target classification or tracking.
- Whilst there being much potential for extension of real time functionality via batches algorithm, the testbed utilised FFT based correlation detection, which prevented real time RDMap processing.

- The testbed configuration was limited to use based on relatively high power, wide bandwidth terrestrial digital signals such as DAB+ and DVB-T, with no testing conducted on other illuminators of opportunity, such as satellite signals or analogue signals.

These limitations come as a result on optimising the testbed design and implementation for low cost, user friendly, and scaleable passive radar detection, with the intention of providing a proof of concept for future development. Moreover, there is an abundance of literature and even commercial products that have addressed these limitations, with the intention of providing a more complete passive radar detection system.

6.3 Possible Future Work

In light of the research and demonstrated proof of concept of this thesis, several recommendations and areas for future work have been identified, both in terms of broad passive bistatic radar and low cost implementations. In terms of low cost implementations and test bed, the logical next steps would be to build off the stated project limitations.

The primary development would be the development and processing of another channel/(s) for multistatic detection, allowing for angle of arrival detection and potentially target tracking. This would require the development of a second RX channel, along with the associated signal processing and detection algorithms, akin to the KrakenSDR product [8], or could potentially even involve the integration of the Kraken into the RPi5 testbed itself.

Another route of development would be the exploration of real time processing and detection algorithms, such as the Batches algorithm, which represent a lower computational intensity than the FFT based correlation detection used in this thesis [32]. Associated with this development would be the possible use of lower compute and subsequently lower cost platforms.

Finally, cluster suppression algorithms could be implemented and even developed to allow for the detection of smaller, further away targets, along with the potential for target classification. This has been shown previously through the implementation of BMS, GMS and CFAR [49]. Noting that these methods are computationally intensive and more signal processing focused as opposed to hardware focused.

Along with the above specific potential development areas, some other general extensions based on the research and design of this thesis include:

- Development of a simple, generic SDR sampling software library / gui to unify the process of obtaining IQ samples in the form of a .bin file.
- Exploration of software to automate the RDMap generation process taking params such as sample rate and the .bin file as inputs.
- Addition of LCD display to testbed for localised data visualisation and control.

Chapter 7

Bibliography

- [1] Ieee standard definitions of terms for antennas. *IEEE Std 145-1993*, pages 1–32, 1993.
- [2] *Introduction to the Internet of Things*, pages 1–50. 2018.
- [3] Adafruit. 16mm illuminated pushbutton, 2024. Accessed: 2024-09-01.
- [4] Australian Communications and Media Authority. Australian radiofrequency spectrum allocations chart, 2019. Accessed: 2024-10-17.
- [5] Christian R. Berger, Bruno Demissie, JÖrg Heckenbach, Peter Willett, and Shengli Zhou. Signal processing for passive radar using ofdm waveforms. *IEEE Journal of Selected Topics in Signal Processing*, 4(1):226–238, 2010.
- [6] Konstanty Bialkowski. Coms4105 prac 1. University of Queensland, 2024. Image retrieved from the assignment sheet.
- [7] Stefan Brisken, Matteo Moscadelli, Viktor Seidel, and Christoph Schwark. Passive radar imaging using dvb-s2. *IEEE*, 2024. Cite This.
- [8] Stephen Cass. Passive radar with the krakensdr > spot stuff with tv antennas and a software-defined radio. *IEEE Spectrum*, 59(11):16–18, 2022.
- [9] C.J. Coleman, R.A. Watson, and H. Yardley. A practical bistatic passive radar system for use with dab and drm illuminators. In *2008 IEEE Radar Conference*, pages 1–6, 2008.
- [10] Core Electronics. Raspberry pi 5 model b (8gb), 2024. Accessed: 2024-09-01.
- [11] Lockheed Martin Corporation. Silent sentry passive surveillance system. Technical report, 2000. Accessed: 2024-10-23.
- [12] Ishan Dhar. Tcp connections and sockets: Deep dive into networking fundamentals with linux and python. <https://medium.com/@dhar.ishan04/tcp-connections-and-sockets-deep-dive-into-networking-fundamentals-with-linux-and-p> 2020. Accessed: 2024-10-08.
- [13] Deepwave Digital. Recording signals tutorial. https://docs.deepwavedigital.com/Tutorials/2_recording_signals/, 2023. Accessed: 2024-09-20.
- [14] Digitek. Digitek 01buwx18l 18 elements outer metro uhf antenna, 2024. Accessed: 2024-10-20.

- [15] Anthony Eden. Digital radio in australia: Dab+ technical overview, 2023. Accessed: 2024-09-02.
- [16] Michael Edrich, Alexander Schroeder, and Fabienne Meyer. Design and performance evaluation of a mature fm/dab/dvb-t multi-illuminator passive radar system. *IET Radar, Sonar & Navigation*, 8(2):114–122, 2014.
- [17] ETSI. En 300 401 - radio broadcasting systems; digital audio broadcasting (dab) to mobile, portable, and fixed receivers. https://www.etsi.org/deliver/etsi_en/300400_300499/300401/02.01.01_60/en_300401v020101p.pdf, 2016. Accessed: 2024-09-02.
- [18] Flightradar24. Build your own ads-b ground station. <https://www.flightradar24.com/build-your-own>, 2024. Accessed: 2024-09-01.
- [19] Vijay K. Garg. Software-defined radio. In *Wireless Communications & Networking*. Elsevier, 2007. Accessed: 2024-08-20.
- [20] Alexander Gillis. Secure shell (ssh), 2023. Accessed: 2024-10-08.
- [21] H. Griffiths, Christopher J. Baker, and Ieee Xplore. *An introduction to passive radar*. Artech House radar series. Artech House IEEE Xplore, Boston Piscataqay, New Jersey, first edition edition, 2017.
- [22] Hugh Griffiths. Chapter 16 - passive bistatic radar. In Nicholas D. Sidiropoulos, Fulvio Gini, Rama Chellappa, and Sergios Theodoridis, editors, *Academic Press Library in Signal Processing: Volume 2*, volume 2 of *Academic Press Library in Signal Processing*, pages 813–855. Elsevier, 2014.
- [23] Abdulkadir Guner. Ambiguity function analysis and direct-path signal filtering of the digital audio broadcast (dab) waveform for passive coherent location (pcl). 2002.
- [24] Tri-Tan Van Cao James Palmer, Simon Palumbo, , and Stephen Howard. A new illuminator of opportunity bistatic radar research project at dsto. Report, Defence Science and Technology Organisation, May 2009 2009.
- [25] Don Koks. How to create and manipulate radar range-doppler plots. Technical Report DSTO-TN-1386, Defence Science and Technology Organisation, Cyber & Electronic Warfare Division, Australian Government, 2012.
- [26] Steve M. librtlsdr, 2024. Accessed: 2024-09-17.
- [27] Osama Mahfoudia, François Horlin, and Xavier Neyt. On the feasibility of DVB-T based passive radar with a single receiver channel. In *Proceedings of the 15th International Radar Symposium (IRS)*, pages 1–6. IEEE, 2014.
- [28] Lockheed Martin. What is a radar band and why is it important?, 2024. Accessed: 2024-10-17.
- [29] J. Mason. Adaptive streaming of high-quality audio over low-bitrate networks, 2024. Accessed: October 20, 2024.
- [30] Filip Michalak, Wojciech Zabołotny, Łukasz Podkalicki, Mateusz Malanowski, Marcin Piasecki, and Krzysztof Kulpa. Universal rfsoc-based signal recorder for radar applications. In *2022 23rd International Radar Symposium (IRS)*, pages 136–140, 2022.

- [31] C. Moscardini, D. Petri, A. Capria, M. Conti, M. Martorella, and F. Berizzi. Batches algorithm for passive radar: a theoretical analysis. *IEEE Transactions on Aerospace and Electronic Systems*, 51(2):1475–1487, 2015.
- [32] Daniel Moser, Giorgio Tresoldi, Christof Schüpbach, and Vincent Lenders. Design and evaluation of a low-cost passive radar receiver based on iot hardware. In *2019 IEEE Radar Conference (RadarConf)*, pages 1–6, April 2019.
- [33] myriadrf. Limesdr-usb, 2024. Accessed: 2024-09-10.
- [34] Avram Piltch. Raspberry pi 5’s wi-fi gets faster. 2024. Accessed: 2024-09-01.
- [35] Pimoroni. Nvme base, 2024. Accessed: 2024-08-20.
- [36] Pothosware. Soapysdr, 2024. Accessed: 2024-09-17.
- [37] Rasmussen and Printables. Raspberry pi 5 case for pimoroni nvme ssd base option, 2024. Accessed: 2024-10-04.
- [38] RTL-SDR.com. Buy rtl-sdr dongles (rtl2832u). <https://www.rtl-sdr.com/buy-rtl-sdr-dvb-t-dongles/>, 2024. Accessed: 2024-03-11.
- [39] Mathew NO Sadiku and Cajetan M Akujuobi. Software-defined radio: a brief overview. *Ieee Potentials*, 23(4):14–15, 2004.
- [40] Dilusha Samarasekara. Popular sdrs, 2023. Accessed: 2024-08-20.
- [41] Christof Schüpbach and Samuel Welschen. Direct signal interference mitigation by slow-time frequency correction for ofdm-based passive radar. In *2018 19th International Radar Symposium (IRS)*, pages 1–10, 2018.
- [42] Joshua Leigh Sendall. Implementation of a low-cost bistatic radar. Master’s thesis, 2016.
- [43] Superkuh. Rtl-sdr, n.d. Accessed: 2024-08-27.
- [44] J. M. Thomas, C. J. Baker, and H. D. Griffiths. Hf passive bistatic radar: Potential and applications for remote sensing. *IEEE Aerospace and Electronic Systems Magazine*, 2005. Cite This, PDF available.
- [45] Martin Ummenhofer, Louis Cesbron Lavau, Diego Cristallini, and Daniel O’Hagan. Uav micro-doppler signature analysis using dvb-s based passive radar. *IEEE*, 2024. Accessed: Oct. 17, 2024.
- [46] Maria V. Vildyaeva, Elizaveta A. Egorova, and Aleksandr B. Vavrenyuk. Using a neural network to convert a radio signal from an rtl-sdr receiver to text. In *2020 IEEE Conference of Russian Young Researchers in Electrical and Electronic Engineering (EICoRus)*, pages 1449–1451, 2020.
- [47] XDA Developers. Best single board computers, 2024. Accessed: 2024-09-01.
- [48] Ying Yin, Shunsheng Zhang, Fuxia Wu, Zhulin Zong, and Wei Zhang. Passive radar detection with dvb-t signals. In *2016 CIE International Conference on Radar (RADAR)*, pages 1–5, 2016.

- [49] Lu Zhang and Konstanty S. Bialkowski. Passive radar for low doppler targets detection using background estimation and subtraction. In *2020 IEEE International Conference on Radar (RADAR)*, pages 1–6, Brisbane, QLD, Australia, 2020. IEEE.

Appendices

Appendix A

Code and Results

A.1 GitHub Repository

The code used throughout this project can be found at the following link.

<https://github.com/flynnmkelly/PassiveRadarThesis/tree/main>

Specifically, the code running via crontab on the Raspberry Pi 5 can be viewed in the *RPi5 Testbed Final* directory.

A.2 Youtube Channel with Demonstration

The links below show the demonstration of the testbed in action, along with some of the GIF RDM output:

www.youtube.com/@flynnkelly5098

Appendix B

System Initialization and Testing

The below sections detail the initial setup and testing of the Raspberry Pi 5 and different SDR hardware modules.

B.1 SoapySDRUtil LimeSDR Probe Output

```
[INFO] Make connection: 'LimeSDR-USB [USB 3.0] 90706024F3821'
libusb: warning [darwin_transfer_status] transfer error: timed out
[INFO] Reference clock 30.72 MHz
[INFO] Device name: LimeSDR-USB
[INFO] Reference: 30.72 MHz
[INFO] LMS7002M register cache: Disabled

-----
-- Device identification
-----
driver=FX3
hardware=LimeSDR-USB
boardSerialNumber=0x90706024f3821
firmwareVersion=4
gatewareVersion=2.23
hardwareVersion=4
protocolVersion=1

-----
-- Peripheral summary
-----
Channels: 2 Rx, 2 Tx
Timestamps: YES
Clock sources: internal, external
Sensors: clock_locked, lms7_temp
  * clock_locked (Clock Locked): true
    CGEN clock is locked, good VCO selection.
  * lms7_temp (LMS7 Temperature): 41.495247 C
    The temperature of the LMS7002M in degrees C.
Registers: BBIC, RFICO
Other Settings:
  * SAVE_CONFIG - Save LMS settings to file
    [key=SAVE_CONFIG, type=string]
  * LOAD_CONFIG - Load LMS settings from file
```

```

[key=LOAD_CONFIG, type=string]
* OVERSAMPLING - oversampling ratio (0 - auto)
  [key=OVERSAMPLING, type=int, options=(0, 1, 2, 4, 8, 16, 32)]
GPIOs: MAIN

-----
-- RX Channel 0
-----

Full-duplex: YES
Supports AGC: NO
Stream formats: CF32, CS12, CS16
Native format: CS16 [full-scale=32767]
Stream args:
* Buffer Length - The buffer transfer size over the link.
  [key=bufferLength, units=samples, default=0, type=int]
* Latency - Latency vs. performance
  [key=latency, default=0.5, type=float]
* Link Format - The format of the samples over the link.
  [key=linkFormat, default=CS16, type=string, options=(CS16, CS12)]
* Skip Calibration - Skip automatic activation calibration.
  [key=skipCal, default=false, type=bool]
* align phase - Attempt to align phase of Rx channels.
  [key=alignPhase, default=false, type=bool]
Antennas: NONE, LNAH, LNAL, LNAW, LB1, LB2
Corrections: DC removal, DC offset, IQ balance
Full gain range: [-12, 61] dB
TIA gain range: [0, 12] dB
LNA gain range: [0, 30] dB
PGA gain range: [-12, 19] dB
Full freq range: [0, 3800] MHz
RF freq range: [30, 3800] MHz
BB freq range: [-10, 10] MHz
Tune args:
* LO Offset - Tune the LO with an offset and compensate with the baseband CORDIC.
  [key=OFFSET, units=Hz, default=0.0, type=float, range=[-1e+07, 1e+07]]
* BB - Specify a specific value for this component or IGNORE to skip tuning it.
  [key=BB, units=Hz, default=DEFAULT, type=float, range=[-1e+07, 1e+07],
   options=(DEFAULT, IGNORE)]
Sample rates: [0.1, 61.44] MSps
Filter bandwidths: [1.4001, 130] MHz
Sensors: lo_locked
* lo_locked (LO Locked): false
  LO synthesizer is locked, good VCO selection.
Other Settings:
* TSP_CONST - Digital DC test signal level in LMS7002M TSP chain.
  [key=TSP_CONST, default=16383, type=int, range=[0, 32767]]
* CALIBRATE - DC/IQ calibration bandwidth
  [key=CALIBRATE, type=float, range=[2.5e+06, 1.2e+08]]
* ENABLE_GFIR_LPF - LPF bandwidth (must be set after sample rate)
  [key=ENABLE_GFIR_LPF, type=float]
* TSG_NCO - Enable NCO test signal
  [key=TSG_NCO, default=4, type=int, options=(-1, 4, 8)]

-----
-- RX Channel 1
-----

Full-duplex: YES
Supports AGC: NO
Stream formats: CF32, CS12, CS16

```

```

Native format: CS16 [full-scale=32767]
Stream args:
  * Buffer Length - The buffer transfer size over the link.
    [key=bufferLength, units=samples, default=0, type=int]
  * Latency - Latency vs. performance
    [key=latency, default=0.5, type=float]
  * Link Format - The format of the samples over the link.
    [key=linkFormat, default=CS16, type=string, options=(CS16, CS12)]
  * Skip Calibration - Skip automatic activation calibration.
    [key=skipCal, default=false, type=bool]
  * align phase - Attempt to align phase of Rx channels.
    [key=alignPhase, default=false, type=bool]
Antennas: NONE, LNAH, LNAL, LNAW, LB1, LB2
Corrections: DC removal, DC offset, IQ balance
Full gain range: [-12, 61] dB
  TIA gain range: [0, 12] dB
  LNA gain range: [0, 30] dB
  PGA gain range: [-12, 19] dB
Full freq range: [0, 3800] MHz
  RF freq range: [30, 3800] MHz
  BB freq range: [-10, 10] MHz
Tune args:
  * LO Offset - Tune the LO with an offset and compensate with the baseband CORDIC.
    [key=OFFSET, units=Hz, default=0.0, type=float, range=[-1e+07, 1e+07]]
  * BB - Specify a specific value for this component or IGNORE to skip tuning it.
    [key=BB, units=Hz, default=DEFAULT, type=float, range=[-1e+07, 1e+07],
     options=(DEFAULT, IGNORE)]
Sample rates: [0.1, 61.44] MSps
Filter bandwidths: [1.4001, 130] MHz
Sensors: lo_locked
  * lo_locked (LO Locked): false
    LO synthesizer is locked, good VCO selection.
Other Settings:
  * TSP_CONST - Digital DC test signal level in LMS7002M TSP chain.
    [key=TSP_CONST, default=16383, type=int, range=[0, 32767]]
  * CALIBRATE - DC/IQ calibration bandwidth
    [key=CALIBRATE, type=float, range=[2.5e+06, 1.2e+08]]
  * ENABLE_GFIR_LPF - LPF bandwidth (must be set after sample rate)
    [key=ENABLE_GFIR_LPF, type=float]
  * TSG_NCO - Enable NCO test signal
    [key=TSG_NCO, default=4, type=int, options=(-1, 4, 8)]

```

-- TX Channel 0

```

Full-duplex: YES
Supports AGC: NO
Stream formats: CF32, CS12, CS16
Native format: CS16 [full-scale=32767]
Stream args:
  * Buffer Length - The buffer transfer size over the link.
    [key=bufferLength, units=samples, default=0, type=int]
  * Latency - Latency vs. performance
    [key=latency, default=0.5, type=float]
  * Link Format - The format of the samples over the link.
    [key=linkFormat, default=CS16, type=string, options=(CS16, CS12)]
  * Skip Calibration - Skip automatic activation calibration.
    [key=skipCal, default=false, type=bool]
  * align phase - Attempt to align phase of Rx channels.

```

```

    [key=alignPhase, default=false, type=bool]
Antennas: NONE, BAND1, BAND2
Corrections: DC offset, IQ balance
Full gain range: [-12, 64] dB
    PAD gain range: [0, 52] dB
    IAMP gain range: [-12, 12] dB
Full freq range: [0, 3800] MHz
    RF freq range: [30, 3800] MHz
    BB freq range: [-10, 10] MHz
Tune args:
    * LO Offset - Tune the LO with an offset and compensate with the baseband CORDIC.
        [key=OFFSET, units=Hz, default=0.0, type=float, range=[-1e+07, 1e+07]]
    * BB - Specify a specific value for this component or IGNORE to skip tuning it.
        [key=BB, units=Hz, default=DEFAULT, type=float, range=[-1e+07, 1e+07],
         options=(DEFAULT, IGNORE)]
Sample rates: [0.1, 61.44] MSps
Filter bandwidths: [5, 40], [50, 130] MHz
Sensors: lo_locked
    * lo_locked (LO Locked): true
        LO synthesizer is locked, good VCO selection.
Other Settings:
    * TSP_CONST - Digital DC test signal level in LMS7002M TSP chain.
        [key=TSP_CONST, default=16383, type=int, range=[0, 32767]]
    * CALIBRATE - DC/IQ calibration bandwidth
        [key=CALIBRATE, type=float, range=[2.5e+06, 1.2e+08]]
    * ENABLE_GFIR_LPF - LPF bandwidth (must be set after sample rate)
        [key=ENABLE_GFIR_LPF, type=float]
    * TSG_NCO - Enable NCO test signal
        [key=TSG_NCO, default=4, type=int, options=(-1, 4, 8)]

```

-- TX Channel 1

```

Full-duplex: YES
Supports AGC: NO
Stream formats: CF32, CS12, CS16
Native format: CS16 [full-scale=32767]
Stream args:
    * Buffer Length - The buffer transfer size over the link.
        [key=bufferLength, units=samples, default=0, type=int]
    * Latency - Latency vs. performance
        [key=latency, default=0.5, type=float]
    * Link Format - The format of the samples over the link.
        [key=linkFormat, default=CS16, type=string, options=(CS16, CS12)]
    * Skip Calibration - Skip automatic activation calibration.
        [key=skipCal, default=false, type=bool]
    * align phase - Attempt to align phase of Rx channels.
        [key=alignPhase, default=false, type=bool]
Antennas: NONE, BAND1, BAND2
Corrections: DC offset, IQ balance
Full gain range: [-12, 64] dB
    PAD gain range: [0, 52] dB
    IAMP gain range: [-12, 12] dB
Full freq range: [0, 3800] MHz
    RF freq range: [30, 3800] MHz
    BB freq range: [-10, 10] MHz
Tune args:
    * LO Offset - Tune the LO with an offset and compensate with the baseband CORDIC.
        [key=OFFSET, units=Hz, default=0.0, type=float, range=[-1e+07, 1e+07]]

```

```

* BB - Specify a specific value for this component or IGNORE to skip tuning it.
  [key=BB, units=Hz, default=DEFAULT, type=float, range=[-1e+07, 1e+07],
   options=(DEFAULT, IGNORE)]
Sample rates: [0.1, 61.44] MSps
Filter bandwidths: [5, 40], [50, 130] MHz
Sensors: lo_locked
  * lo_locked (LO Locked): true
    LO synthesizer is locked, good VCO selection.
Other Settings:
  * TSP_CONST - Digital DC test signal level in LMS7002M TSP chain.
    [key=TSP_CONST, default=16383, type=int, range=[0, 32767]]
  * CALIBRATE - DC/IQ calibration bandwidth
    [key=CALIBRATE, type=float, range=[2.5e+06, 1.2e+08]]
  * ENABLE_GFIR_LPF - LPF bandwidth (must be set after sample rate)
    [key=ENABLE_GFIR_LPF, type=float]
  * TSG_NCO - Enable NCO test signal
    [key=TSG_NCO, default=4, type=int, options=(-1, 4, 8)]

```

Listing B.1: SoapySDRUtil Probe Output for LimeSDR

B.2 SoapySDRUtil RTL-SDR Probe Output

```

Found Rafael Micro R828D tuner
[INFO] Opening Generic RTL2832U OEM :: 00000001...
Found Rafael Micro R828D tuner

-----
-- Device identification
-----
driver=RTLSDR
hardware=R828D
index=0
origin=https://github.com/pothosware/SoapyRTLSDR

-----
-- Peripheral summary
-----
Channels: 1 Rx, 0 Tx
Timestamps: YES
Time sources: sw_ticks
Other Settings:
  * Direct Sampling - RTL-SDR Direct Sampling Mode
    [key=direct_samp, default=0, type=string, options=(0, 1, 2)]
  * Offset Tune - RTL-SDR Offset Tuning Mode
    [key=offset_tune, default=false, type=bool]
  * I/Q Swap - RTL-SDR I/Q Swap Mode
    [key=iq_swap, default=false, type=bool]
  * Digital AGC - RTL-SDR digital AGC Mode
    [key=digital_agc, default=false, type=bool]
  * Bias Tee - RTL-SDR Blog V.3 Bias-Tee Mode
    [key=biastee, default=false, type=bool]

-----
-- RX Channel 0

```

```
-----
Full-duplex: NO
Supports AGC: YES
Stream formats: CS8, CS16, CF32
Native format: CS8 [full-scale=128]
Stream args:
    * Buffer Size - Number of bytes per buffer, multiples of 512 only.
        [key=bufflen, units=bytes, default=262144, type=int]
    * Ring buffers - Number of buffers in the ring.
        [key=buffers, units=buffers, default=15, type=int]
    * Async buffers - Number of async usb buffers (advanced).
        [key=asyncBuffs, units=buffers, default=0, type=int]
Antennas: RX
Full gain range: [0, 49.6] dB
    TUNER gain range: [0, 49.6] dB
Full freq range: [23.999, 1764] MHz
    RF freq range: [24, 1764] MHz
    CORR freq range: [-0.001, 0.001] MHz
Sample rates: [0.225001, 0.3], [0.900001, 3.2] MSps
Filter bandwidths: [0, 8] MHz
```

Listing B.2: SoapySDRUtil Probe Output for RTL-SDR

B.3 Crontab Configuration

```
flynnmkelly@raspberrypi:~ $ sudo crontab -l
# Edit this file to introduce tasks to be run by cron.
#
# Each task to run has to be defined through a single line
# indicating with different fields when the task will be run
# and what command to run for the task
#
# To define the time you can provide concrete values for
# minute (m), hour (h), day of month (dom), month (mon),
# and day of week (dow) or use '*' in these fields (for 'any').
#
# Notice that tasks will be started based on the cron's system
# daemon's notion of time and timezones.
#
# Output of the crontab jobs (including errors) is sent through
# email to the user the crontab file belongs to (unless redirected).
#
# For example, you can run a backup of all your user accounts
# at 5 a.m every week with:
# 0 5 * * 1 tar -zcf /var/backups/home.tgz /home/
#
# For more information see the manual pages of crontab(5) and cron(8)
#
# m h dom mon dow command
@reboot sh /home/flynnmkelly/Desktop/Testbed/launcher.sh
    >/home/flynnmkelly/logs/cronlog 2>&1
```

Listing B.3: Crontab Configuration for Raspberry Pi